

# An upscaling method for top-systems with layered heterogeneity and vertical anisotropy

David A. Brakenhoff

Technische Universiteit Delft

# An upscaling method for top-systems with layered heterogeneity and vertical anisotropy

by

**David Allan Brakenhoff**

in partial fulfillment of the requirements for the degree of

**Master of Science**  
in Civil Engineering

at the Delft University of Technology.

Student number: 1319353

Thesis committee:	Dr. ir. M. Bakker	TU Delft
	Prof. dr. ir. T. N. Olsthoorn	TU Delft
	Dr. ir. W. J. Zaadnoordijk	KWR & TU Delft
	Prof. dr. ir. T. J. Heimovaara	TU Delft

An electronic version of this thesis is available at  
<http://repository.tudelft.nl/>.

## Summary

The subsurface in the Western part of the Netherlands is generally characterized as a regional aquifer, in which most of the lateral groundwater flow takes place, covered by a semi-permeable layer. The semi-permeable layer is often split into a phreatic layer on top of an aquitard (which has an even lower permeability). The phreatic layer and aquitard together are referred to as the top-system. The phreatic layer contains ditches and drains that transport excess water out of the area to, for example, a belt canal or a river.

In regional groundwater models upscaling methods are applied to replace the top-system by a linear head-flux relationship (a Cauchy boundary condition) to take into account the interaction between many small surface water features and the groundwater in a lumped fashion. The upscaled system contains two parameters: the effective water level and the effective resistance. The geology of the phreatic layer has a large influence on the value of these parameters, but existing upscaling methods are limited to homogeneous and isotropic phreatic layers.

New formulas are derived for the effective parameters that take into account layered heterogeneity and vertical anisotropy. This multi-layer upscaling method is compared to an existing method, derived by [de Lange \(1999\)](#) “A Cauchy boundary condition for the lumped interaction between an arbitrary number of surface waters and a regional aquifer”, *Journal of Hydrology* 266 (1999) (p. 250-261), which does not incorporate these aspects directly. Two upscaled models are created using these two upscaling methods and are compared to an analytic element model containing all features explicitly. The comparison is carried out for a cross-section with an extraction in the regional aquifer.

In homogeneous isotropic phreatic layers both upscaling methods perform well. The drawdown in the regional aquifer differs by less than 3% as compared to the drawdown in the explicit model. When heterogeneity and anisotropy are introduced to the phreatic layer, the multi-layer method performs better with differences in drawdown remaining below 1%. The method by de Lange shows differences of up to 15%. The values of the effective parameters calculated by both models are similar in heterogeneous top-systems characterized by larger phreatic transmissivities, although the multi-layer method is almost always more accurate. For phreatic layers with smaller transmissivities, the multi-layer method yields significantly better estimates for the effective parameters.

The new method does have limitations. It is less accurate in situations where surface water features are wide relative to the distance between them or when the bed resistance of the surface water features is large relative to

the resistance of the aquitard. De Lange's approach is, in theory, applicable under those conditions, but does not take into account heterogeneity or vertical anisotropy. For most practical purposes, the multi-layer upscaling method is preferred and yields similar or more accurate results than de Lange's method.

# Contents

<b>1</b>	<b>Introduction</b>	<b>1</b>
<b>2</b>	<b>Upscaling methods for the top-system</b>	<b>5</b>
2.1	The conceptual model . . . . .	5
2.2	Solution by de Lange . . . . .	7
2.2.1	Approximations . . . . .	8
2.2.2	Accounting for two-dimensional effects . . . . .	9
2.3	A multi-layer upscaling method taking into account anisotropy and heterogeneity . . . . .	10
2.3.1	Derivation of $p^*$ . . . . .	10
2.3.2	Derivation of $c^*$ . . . . .	16
2.3.3	Approximations . . . . .	19
<b>3</b>	<b>Analytic element modeling of multi-aquifer flow</b>	<b>21</b>
3.1	Multi-layer analytic element modeling . . . . .	21
3.2	Derivation of analytic solutions for elements in a multi-layer cross-sectional model . . . . .	22
3.2.1	Setting up and solving the differential equation without areal recharge . . . . .	22
3.2.2	Ditch element with given discharge . . . . .	25
3.2.3	Ditch element with given head . . . . .	27
3.2.4	Head-specified ditch element with bed resistance . . . . .	27
3.2.5	No-flow boundary element . . . . .	29
3.2.6	Areal infiltration . . . . .	29
<b>4</b>	<b>Comparison of upscaling methods for homogeneous phreatic layers</b>	<b>33</b>
4.1	Flow through homogeneous phreatic layers . . . . .	33
4.2	Description of model set-up . . . . .	34
4.3	Performance of upscaling methods . . . . .	36
4.3.1	Scenario 1 . . . . .	37
4.3.2	Scenario 2 . . . . .	38
4.3.3	Scenario 3 . . . . .	38

4.4	Discussion . . . . .	39
<b>5</b>	<b>Comparison of upscaling methods for phreatic layers with layered heterogeneity</b>	<b>41</b>
5.1	Flow through heterogeneous phreatic layers . . . . .	41
5.2	Description of model set-up . . . . .	42
5.3	Performance of upscaling methods for phreatic layers with layered heterogeneity . . . . .	43
5.3.1	Scenario 4 . . . . .	43
5.3.2	Scenario 5 . . . . .	44
5.3.3	The effect of layered heterogeneity on effective parameter values . . . . .	45
5.3.4	Sensitivity of drain pumping rate to a prescribed head	47
5.3.5	The effect of semi-random ditch spacing on the effective parameters . . . . .	48
5.4	Discussion . . . . .	50
<b>6</b>	<b>Limitations of the multi-layer upscaling method</b>	<b>52</b>
6.1	Resistance of the aquitard . . . . .	52
6.2	Recharge . . . . .	54
6.3	Bed resistance of ditches . . . . .	54
<b>7</b>	<b>Discussion and conclusions</b>	<b>57</b>
	<b>References</b>	<b>59</b>
	<b>Appendices</b>	<b>61</b>
<b>A</b>	<b>De Lange’s derivation of the Cauchy boundary condition</b>	<b>61</b>
A.1	The differential equations and boundary conditions . . . . .	61
A.2	Solution of the differential equations and calculating constants	65
A.3	Flux from regional aquifer to the top system per region . . . .	69
A.3.1	Lumped parameters for area between $0 \leq x \leq L/2$ . . . .	69
A.3.2	Lumped parameters for stretch between $-B/2 \leq x \leq 0$	72
A.4	Total flux between regional aquifer and ditches . . . . .	74
<b>B</b>	<b>A cross-sectional analytic element model environment in Python</b>	<b>76</b>
B.1	The Model and AquiferData classes . . . . .	76
B.2	The Element base class and Ditch class . . . . .	79
B.3	The HeadDitch and HeadEquation classes . . . . .	80

# List of Figures

1.1	An aerial photograph of a Dutch polder near the town of Wilnis showing a drainage system with many small ditches. . . . .	1
1.2	A conceptual model of the subsurface. The top system is split into a phreatic layer modeled as a phreatic aquifer and an aquitard. . . . .	2
1.3	The conceptual model in (a) shows a typical phreatic layer. The model in (b) is a simple conceptual model with a fixed water depth on top of a resistance layer. Upscaling methods allow areas with many small surface water features (a) to be translated into a much simpler model (b). . . . .	3
2.1	Conceptual model of the top groundwater system. Source: de Lange (1999). . . . .	6
2.2	Schematization of the Cauchy boundary condition . . . . .	6
2.3	Conceptual model for the derivation of the effective parameters in the Cauchy boundary condition. Source: de Lange (1999). . . . .	7
2.4	Conceptual model for derivation of a new formula for $p^*$ . The dotted line in the top sub-layer signifies a ditch, the solid lines represent no-flow boundaries. . . . .	11
2.5	Conceptual model for derivation of a new formula for $c^*$ . The dotted line in the first sub-layer is a ditch, the solid lines represent no-flow boundaries. The bottom of the model is permeable. . . . .	17
3.1	Aquifer system definition. . . . .	23
4.1	Streamlines for a clayey homogeneous phreatic layer (the vertical dimension is exaggerated 10 $\times$ ). . . . .	34
4.2	Conceptualizations of the explicit model (a) and the upscaled model (b) with a drain in the regional aquifer with pumping rate $Q_w$ . . . . .	35
4.3	Conceptual model of the subsurface. . . . .	35

4.4	Groundwater head in the regional aquifer for the explicit model and both upscaled models for Scenario 2 with $Q_w = 1.0$ m <sup>2</sup> /d. . . . .	38
4.5	Groundwater head in the regional aquifer for the explicit model and both upscaled models for Scenario 3 with $Q_w = 1.0$ m <sup>2</sup> /d. . . . .	39
5.1	Streamlines for a heterogeneous phreatic layer with sand, clay and clay sub-layers from top to bottom. The vertical dimension is exaggerated 10×. . . . .	42
5.2	Streamlines for heterogeneous phreatic layer with clay, sand and peat sub-layers from top to bottom. The vertical dimension is exaggerated 10×. . . . .	42
5.3	Streamlines for heterogeneous phreatic layer with clay, clay and sand sub-layers from top to bottom. The vertical dimension is exaggerated 10×. . . . .	43
5.4	Streamlines in a heterogeneous phreatic layer with ten sub-layers. The vertical dimension is exaggerated 10×. . . . .	43
5.5	Heterogeneous lithology of the phreatic layer in Scenarios 4 and 5. The horizontal hydraulic conductivities for clay, peat and sand are 1, 5 and 25 m/d respectively. . . . .	44
5.6	Comparison of the two upscaling methods for $p^*$ for all possible lithologies of a phreatic layers consisting of 3 sub-layers. Note that the lines connecting the points are only included as a visual aid. . . . .	46
5.7	Comparison of the two upscaling methods for $c^*$ for all possible lithologies of a phreatic layer consisting of 3 sub-layers. Note that the lines between the points are only included as a visual aid. . . . .	47
5.8	Pumping rates calculated for a fixed head in the drain for different phreatic layer schematizations with different values for aquitard resistance. Note that the lines between points are only included as a visual aid. . . . .	48
5.9	Head in the regional aquifer for the explicit model, and the two upscaled models for semi-random ditch spacing. The distance between subsequent ditches was randomly selected from 50, 100 or 200 m. The figure on the left was calculated for homogeneous conditions, the one on the right for heterogeneous conditions. . . . .	49

6.1	Comparison of the two upscaling formulas for $p^*$ in isotropic conditions (a) and anisotropic conditions (b) for all possible lithologies of a phreatic layers consisting of 3 sub-layers with $c_1 = 0$ d. Note that the lines connecting the points are only included as a visual aid. . . . .	53
6.2	Comparison of the two upscaling formulas for $c^*$ for all possible lithologies of a phreatic layers consisting of 3 sub-layers with $R = 0.01$ m/d. Note that the lines connecting points are only included as a visual aid. . . . .	54
6.3	Comparison of the two upscaling formulas for $p^*$ for all possible lithologies of a phreatic layers consisting of 3 sub-layers with $c_0 = 1$ d. Note that the lines connecting points are only included as a visual aid. . . . .	55
A.1	All fluxes flowing into and out of an element with width $\Delta x$ in the stretch $-B/2 \leq x \leq 0$ . . . . .	62
A.2	Schematizations of the fluxes through the leaky layers. . . . .	63
A.3	All fluxes for an element with width $\Delta x$ in the stretch $0 \leq x \leq L/2$ . . . . .	64

# List of Tables

4.1	Parameter values describing the subsurface and layout of ditches in the explicit model (see Figure 4.3). . . . .	34
4.2	Description of the schematization of the phreatic layer for the explicit model. The upscaled models are tested against the explicit model for each scenario. . . . .	36
4.3	Drawdown comparison for all scenarios for three points in the cross-section. A value of 1.0 indicates a perfect correspondence between the drawdown calculated by the explicit model and the upscaled model. . . . .	37
4.4	Values for effective parameters $p^*$ and $c^*$ for Scenarios 1-3. The values for the explicit model were determined with an optimization. . . . .	38
5.1	Description of the schematization of the phreatic layer for the explicit model. The simplified models are tested against the explicit model for each scenario. . . . .	44
5.2	Drawdown comparison for Scenario 4 and 5 for three observation points in the cross-section. A value of 1.0 indicates a perfect correspondence between the drawdown calculated by the explicit model and the upscaled model. . . . .	45
5.3	Values for effective parameters $p^*$ and $c^*$ for Scenarios 4 and 5. The values for the explicit model were determined with an optimization. . . . .	45

# Chapter 1

## Introduction

In groundwater models it is important to accurately quantify the interaction between groundwater and surface water. In delta regions such as the Netherlands, a complex drainage network consisting of drains, ditches, and rivers transports excess water to the sea. Within this drainage network different levels can be discerned; the largest features are the major rivers flowing to the sea, the smallest surface water components are the ditches that keep a polder from flooding.



**Figure 1.1:** An aerial photograph of a Dutch polder near the town of Wilnis showing a drainage system with many small ditches.

The larger surface water features are easily included in regional groundwater models as there are only a few of them and their impact on groundwater flow in the regional aquifer is large (de Lange, 1996). Conversely, the smaller features are large in number and have a small impact individually. However, taken together, their influence on groundwater flow is substantial

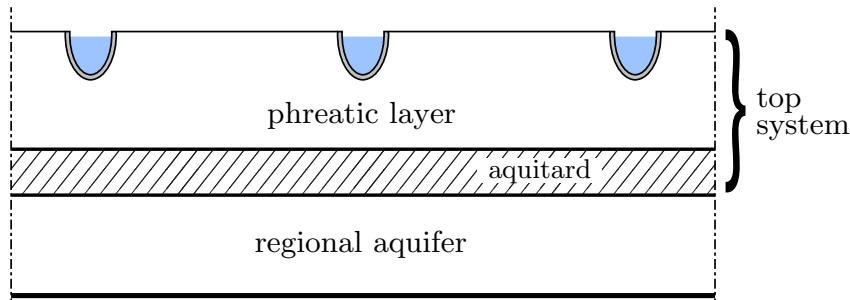


**Figure 1.2:** A conceptual model of the subsurface. The top system is split into a phreatic layer modeled as a phreatic aquifer and an aquitard.

but including all of them individually in a groundwater model is unfeasible. The computation time required to solve such a model would be large and severely limit the model’s practical use ([Ad hoc Werkgroep Consensus Hydrologie, 2002](#)). Scientists (e.g. [van Drecht, 1983](#); [Ernst, 1962](#); [Kovar and Rolf, 1978](#); [de Lange, 1996](#); [Maas, 2008](#)) have tackled this problem by developing methods to lump smaller features together in regional groundwater models.

One such method was developed by [de Lange \(1996\)](#) and has since been implemented in the groundwater model part of the NHI (Nationaal Hydrologisch Instrument), a national hydrological model for the Netherlands ([Vergroesen et al., 2008](#)). By lumping smaller features, their impact on groundwater flow can be included in regional models without greatly increasing the required computation time. This approach is known as upscaling. Though detail is lost in this process, the magnitude of the interaction between regional groundwater and surface water is preserved.

The geology of the subsurface is an important aspect in determining the magnitude of this interaction. The subsurface in the Western part of the Netherlands is characterized by Holocene deposits on top of a regional aquifer consisting of Pleistocene sand (e.g. [Dufour, 2000](#)). The Holocene layer is highly heterogeneous and complex, consisting mostly of peat and clay but also sandy deposits (e.g. [Sutanudjaja, 2008](#)). In conceptual groundwater models this layer is often separated into a phreatic aquifer (also referred to as the phreatic layer) on top of an aquitard (Figure 1.2). The phreatic aquifer together with the aquitard form the top system.

The upscaling method by [de Lange](#) replaces the top system, and all the surface water features it contains by a single semi-permeable layer, covered by a fixed water level (Figure 1.3). The water level is equal to an effective average groundwater head in the phreatic layer. The semi-permeable layer accounts for the effective resistance to groundwater flow through the top system. The goal of upscaling is to estimate the value of the effective

average groundwater level (denoted by  $p^*$ ) and the effective resistance of the top system (denoted by  $c^*$ ) from measurable physical characteristics of the subsurface such that the flux between groundwater and surface water is preserved.

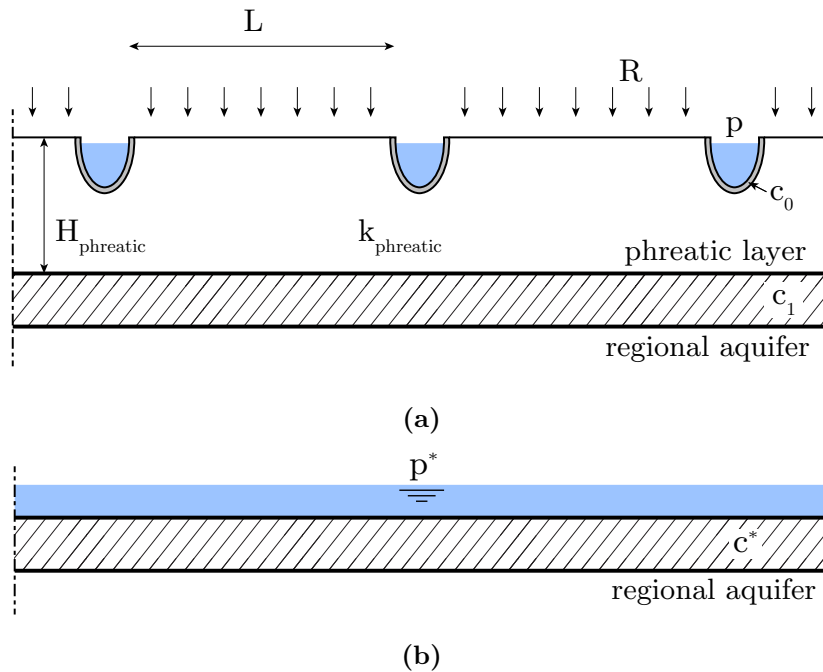


**Figure 1.3:** The conceptual model in (a) shows a typical phreatic layer. The model in (b) is a simple conceptual model with a fixed water depth on top of a resistance layer. Upscaling methods allow areas with many small surface water features (a) to be translated into a much simpler model (b).

De Lange (1999) derived expressions for  $p^*$  and  $c^*$  based on a set of approximations. Two of the most interesting approximations are that the phreatic layer is homogeneous and isotropic and that ditches lie on top of the phreatic layer (the ditches do not penetrate the phreatic layer). In reality, the phreatic layer rarely meets these conditions (Sutanudjaja, 2008). De Lange (1999) proposes several methods to take into account the influence of phreatic layers that deviate from the idealized one used to derive expressions for  $p^*$  and  $c^*$ . One addition is the inclusion of the radial resistance as described by Ernst (1962) to account for two-dimensional effects due to the partial penetration of surface water features. These methods do not take into account anisotropy or heterogeneity of the phreatic layer.

This report aims to answer the following questions:

1. How can partial penetration of surface water features, vertical anisotropy and layered heterogeneity be accounted for directly in the

formulas for  $p^*$  and  $c^*$ ?

2. How does such a new upscaling method compare with the method derived by [de Lange \(1999\)](#) and a model containing all surface water features explicitly for different complex phreatic layer schematizations?

To answer the first research question, new schematizations of the phreatic layer that account for anisotropy and heterogeneity are defined and solved. The phreatic layers in these schematizations consist of multiple sub-layers. These multi-layer conceptual models are solved to derive new formulas for parameters  $p^*$  and  $c^*$ .

The second question is answered by comparing a model in which all features (e.g. ditches) are included explicitly (referred to as the explicit model) to two upscaled models, one defined by the multi-layer method and one by the method of [de Lange \(1999\)](#). In the upscaled models all the surface waters features in the explicit model and the top-system are replaced by an effective water level on top of an effective resistance layer. Several explicit models are created with increasingly complex conceptualizations of the phreatic layer. Comparisons are made between the heads in the regional aquifer calculated by the different models near an extraction in the regional aquifer to assess the performance of the upscaling methods. The models are created in a multi-layer analytic element modeling environment for cross-sectional flow.

Chapter 2 describes the upscaling method for the subsurface presented by [de Lange \(1999\)](#) and the derivation of the new formulas for  $p^*$  and  $c^*$  based on the multi-layer upscaling method. The analytic functions implemented in the analytic element model environment used to assess the upscaling methods are derived in Chapter 3. Chapters 4 and 5 present and discuss the results of the comparison between the two upscaling methods and the explicit model for homogeneous and heterogeneous phreatic layers, respectively. In Chapter 6, analysis of the approximations used in the derivation of the multi-layer upscaling method is presented, including the limitations of the multi-layer method. Chapter 7 contains the conclusions of this report and gives recommendations for further research.

## Chapter 2

# Upscaling methods for the top-system

Two methods are presented to parametrize the top-system. In this upscaling process, the interaction between the regional aquifer and the surface water features in the phreatic layer is captured by two parameters, the effective water level  $p^*$  and the effective resistance  $c^*$ . The basic principle of upscaling and the conceptual model are presented in Section 2.1. The first method, based on de Lange (1996, 1997a, 1999), is described briefly in Section 2.2 (a more detailed derivation is presented in Appendix A). In Section 2.3, a new method is proposed that takes into account vertical anisotropy and layered heterogeneity of the phreatic layer directly.

### 2.1 The conceptual model

The subsurface in the Western part of the Netherlands is commonly schematized as a regional aquifer separated from a semi-permeable layer by an aquitard (Figure 2.1). The semi-permeable layer is often a phreatic aquifer that contains many small surface water features.

All these drains, ditches and surface water features are combined in a linear head-flux boundary condition that lumps the effects of all these features (see Figure 1.3). This linear relationship between the head and its derivative (the flux) is known as a Cauchy boundary condition and can be written as

$$s = \frac{(h - p^*)}{c^*} \quad (2.1)$$

where  $s$  is a flux,  $h$  represents the head in the regional aquifer, and  $p^*$  is the effective water level on top of the semi-permeable layer with resistance  $c^*$  (Bear in de Lange, 1999). Figure 2.2 portrays the Cauchy boundary condition conceptually.

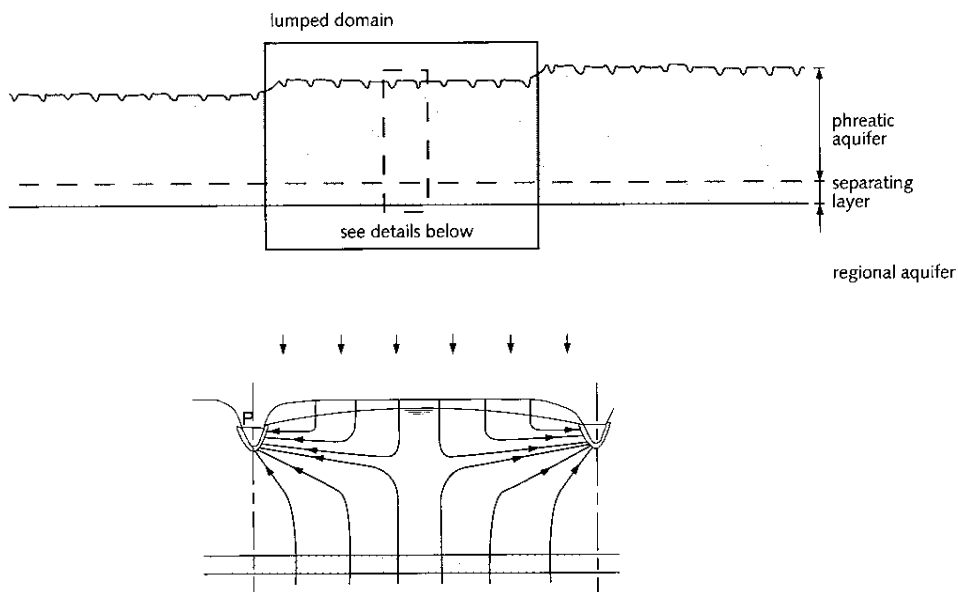


**Figure 2.1:** Conceptual model of the top groundwater system. Source: [de Lange \(1999\)](#).

The objective of the upscaling method is to find expressions for the effective parameters  $p^*$  and  $c^*$  based on measurable physical parameters. Some detail is lost in the upscaling process, of course, but on a regional scale the model should yield accurate results: the flux from the regional aquifer to surface water in the simplified model should be a good approximation of the sum of the actual fluxes to or from the many different surface water features that are present in reality.

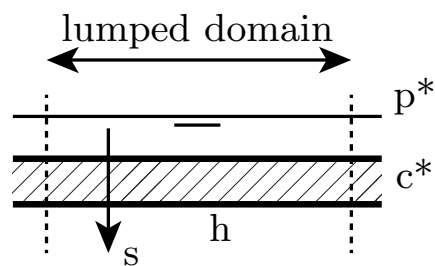


**Figure 2.2:** Schematization of the Cauchy boundary condition

## 2.2 Solution by de Lange

The conceptual model used by de Lange to derive expressions for the effective parameters in the Cauchy boundary condition is shown in Figure 2.3. It consists of a phreatic aquifer bounded at the bottom by an aquitard with resistance  $c_1$ . Assuming symmetry of flow means there are water divides halfway between two ditches and at the midpoint of a ditch. The point at the right boundary of the ditch is defined as  $x = 0$ . The model boundaries are  $-B/2$  and  $L/2$  where  $B$  is the width of a ditch and  $L$  is the distance between two ditches.

The ditch has water level  $p$  and a bed resistance  $c_0$ . The head in the regional aquifer is assumed constant and is represented by  $\phi$ . The head in the phreatic aquifer is denoted by  $h$ . In the region where  $x \geq 0$  there is recharge with magnitude  $R$  (positive for water entering the system).

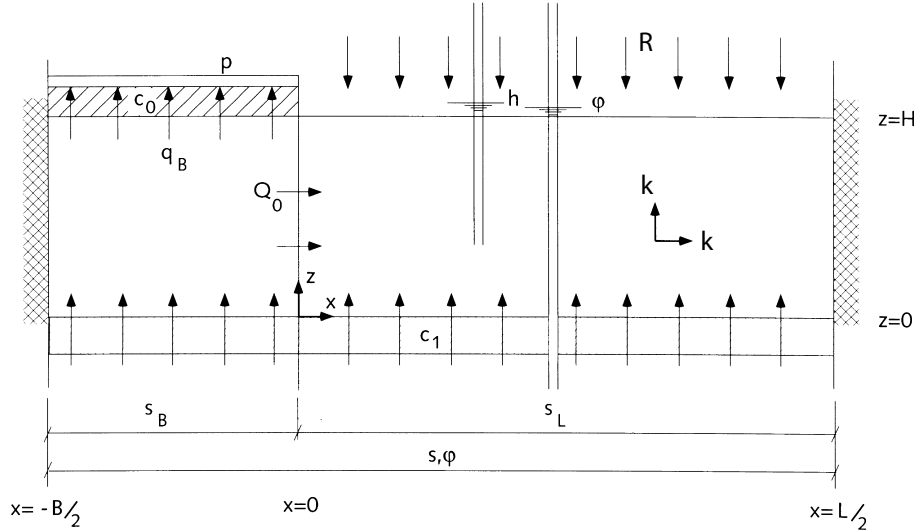


**Figure 2.3:** Conceptual model for the derivation of the effective parameters in the Cauchy boundary condition. Source: [de Lange \(1999\)](#).

De Lange derived formulas for the effective parameters by solving the differential equations governing groundwater flow for the region under a ditch and the region between ditches separately, and subsequently combining the solutions to calculate the total flux through the top system. First the one dimensional differential equations are derived for the region between ditches ( $0 \leq x \leq \frac{L}{2}$ ), and the area under a ditch ( $-\frac{B}{2} \leq x \leq 0$ ). The average fluxes are calculated for each stretch and combined to get a final solution for the total flux to the surface water features. The expressions for the effective parameters  $p^*$  and  $c^*$ , (Eq. 2.2) and (Eq. 2.3), can be found from the formula for the total flux.

$$p^* = p + \frac{RL(c_0 + c_1)(c_L^* - c_1)}{Bc_L^* + Lc_1} \quad (2.2)$$

$$c^* = \frac{(B + L)(c_0 + c_1)c_L^*}{Bc_L^* + Lc_1} \quad (2.3)$$

with

$$c_L^* = (c_0 + c_1) \frac{L}{2\lambda_L} \coth\left(\frac{L}{2\lambda_L}\right) + \frac{Lc_0}{B} \frac{B}{2\lambda_B} \coth\left(\frac{B}{2\lambda_B}\right) \quad (2.4)$$

$$\lambda_L = \sqrt{kHc_1}$$

$$\lambda_B = \sqrt{\frac{kHc_0c_1}{c_1 + c_0}}$$

$p$  - water level in ditch [L]

$R$  - recharge, positive for water entering the system [L/T]

$L$  - distance between two ditches [L]

$B$  - width of a ditch [L]

$c_0$  - bed resistance of the ditch [T]

$c_1$  - resistance of the aquitard separating the regional aquifer from the phreatic layer [T]

$k$  - hydraulic conductivity in the phreatic layer [L/T]

$H$  - thickness of the phreatic layer [L]

### 2.2.1 Approximations

[De Lange \(1999\)](#) made the following approximations to simplify the sub-surface so that it can be solved using simple one-dimensional differential equations and boundary conditions:

- The Dupuit-Forchheimer approximation is adopted. The head is constant along a vertical profile and the horizontal water velocity is constant over the depth.
- The ditches are equidistant, parallel and infinitely long. This approximation along with the Dupuit-Forchheimer approximation simplifies the problem to one-dimensional flow.
- There is symmetry of flow, which means there is a water divide in the middle between two ditches and in the middle under a ditch.

- The groundwater recharge is constant in space and time between two ditches.
- The transmissivity is constant in both aquifers.
- The transmissivity of the regional aquifer is much larger than the transmissivity of the phreatic aquifer. This means changes in head in the regional aquifer are likely to be small compared to changes in the phreatic layer allowing the head in the regional aquifer to be approximated as constant.
- The saturated thickness of the phreatic aquifer does not vary and is equal to the saturated thickness of the phreatic aquifer under a ditch.

### 2.2.2 Accounting for two-dimensional effects

De Lange’s upscaling method is based on a one-dimensional conceptual model. If a situation in reality differs strongly from this conceptual model, i.e. ditches that partially penetrate the phreatic layer or the resistance to vertical flow in the phreatic layer cannot be neglected, 2-D effects are introduced that cannot be accounted for in the model directly. De Lange presents methods to account for these effects without altering the conceptual model.

The Dupuit-Forchheimer approximation neglects resistance to vertical flow. If in reality, this resistance is not negligible, it can be accounted for in the upscaling method by adding the extra resistance to the resistance of the aquitard separating the phreatic layer from the regional aquifer. Instead of using  $c_1$  in the formulas, the following resistance is used:

$$c'_1 = c_1 + \frac{H}{k_{z,eq}} \quad (2.5)$$

where  $k_{z,eq}$  is equal to the equivalent vertical hydraulic conductivity calculated with

$$k_{z,eq} = \frac{\sum_{i=1}^N D_i k_{z,i}}{H} \quad (2.6)$$

where  $D_i$  is the thickness of sub-layer  $i$  with vertical resistance  $k_{z,i}$ .

The conceptual model does not account for the extra resistance to flow caused by a ditch that partially penetrates the phreatic layer. To account for this effect [de Lange](#) adds a parameter called the radial resistance to the calculation of the modified resistance layer between two ditches ( $c_L^*$ ). The radial resistance, as explained by [Ernst \(1962\)](#), is the added resistance groundwater flow experiences due to the ditch penetration depth not being equal to the thickness of the aquifer. The convergence of streamlines near a ditch increases the resistance to flow. [Ernst \(1962\)](#) derived a formula for

the radial resistance in an isotropic aquifer based on the distance between ditches  $L$ , the width of the ditches  $B$ , the thickness of the aquifer  $H$ , and the hydraulic conductivity  $k$ :

$$c_{\text{rad}} = \frac{L}{\pi k} \ln \left( \frac{4H}{\pi B} \right) \quad (2.7)$$

In anisotropic conditions the problem is scaled so that it can be solved using the formula above. Instead of the horizontal hydraulic conductivity, the transformed hydraulic conductivity is used:  $\bar{k} = \sqrt{k_x k_z}$  where  $k_x$  and  $k_y$  represent the horizontal and vertical hydraulic conductivity respectively. The vertical dimensions are scaled by a factor  $\sqrt{k_x/k_z}$ . The formula for the radial resistance in an anisotropic aquifer, as given by [Maas \(2008\)](#); [van Drecht \(1997\)](#), is

$$c_{\text{rad}} = \frac{L}{\pi \sqrt{k_x k_z}} \ln \left( \frac{4H \sqrt{k_x}}{\pi B \sqrt{k_z}} \right) \quad (2.8)$$

De Lange adds this term to the effective resistance between two ditches,  $c_L^*$  (Eq. 2.4). There is no physical justification for the addition of the radial resistance to this formula. The optimal place to add this term was determined through a systematic comparison of where it yielded the best results compared to a two-dimensional solution ([de Lange, 1999](#)).

The inclusion of  $c_1'$  (Eq. 2.5) accounts for resistance to vertical flow in the phreatic layer. Addition of the radial resistance  $c_{\text{rad}}$  accounts for the effects of partially penetrating ditches. Finally, including both these terms should make this method applicable to anisotropic phreatic layers ([de Lange, 1999](#)).

## 2.3 A multi-layer upscaling method taking into account anisotropy and heterogeneity

In this section, new equations for the effective parameters  $p^*$  and  $c^*$  are derived that take into account layered heterogeneity and vertical anisotropy.

### 2.3.1 Derivation of $p^*$

A more detailed conceptual model of the top system is solved analytically to derive an expression for the average head in the phreatic layer. Recall that  $p^*$  is equal to the average head between two ditches. A model is created and solved for a situation with a phreatic layer consisting of 3 sub-layers. The final solution will be generalized to work for  $N$  sub-layers at the end of this section.

The new conceptual model is shown in [Figure 2.4](#). In sub-layer 1 there is a ditch with a known water level at  $x = L/2$ . The transmissivity of sub-layer  $i$  is  $T_i$ . Above each sub-layer  $i$  is a leaky layer with zero thickness and

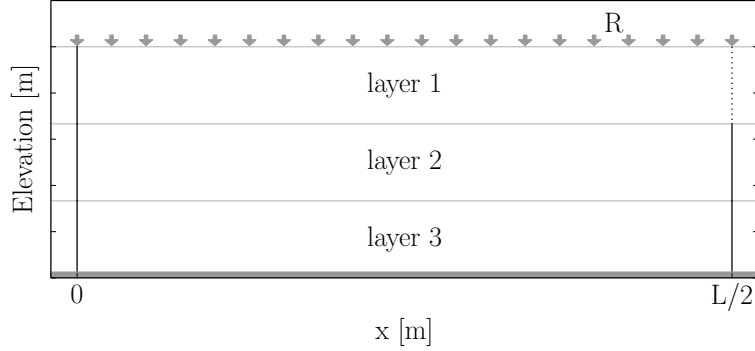


**Figure 2.4:** Conceptual model for derivation of a new formula for  $p^*$ . The dotted line in the top sub-layer signifies a ditch, the solid lines represent no-flow boundaries.

resistance  $c_i$ . The resistance of the leaky layer at the bottom of the phreatic layer ( $c_4$ ) is assumed to be infinite, i.e. it is impermeable. This is not the case in reality, but as long as the flux between the regional aquifer and the phreatic layer is small this approximation will not lead to large errors in the calculation of  $p^*$ . The limits of this approximation will be examined further in Chapter 6. On the right, in sub-layers 2 and 3 there are no-flow boundaries, representing a water divide under the ditch. On the left at  $x = 0$  there is a water divide also modeled with no-flow boundaries in each sub-layer. The water divides signify there are an infinite number of ditches separated by distance  $L$ . The recharge is given by  $R$  in m/d (positive for water entering the system).

The system of differential equations governing the flow is written in terms of potentials and in matrix form. For a more general derivation of the differential equation and its solution, refer to Section 3.2 in the next chapter.

$$\nabla^2 \vec{\Phi} = \begin{pmatrix} \frac{1}{T_1 c_1} + \frac{1}{T_1 c_2} & \frac{-1}{T_2 c_2} & 0 \\ \frac{-1}{T_1 c_2} & \frac{1}{T_2 c_2} + \frac{1}{T_2 c_3} & \frac{-1}{T_3 c_3} \\ 0 & \frac{-1}{T_2 c_3} & \frac{1}{T_3 c_3} \end{pmatrix} \vec{\Phi} + \begin{pmatrix} -R \\ 0 \\ 0 \end{pmatrix} \quad (2.9)$$

where

$$\Phi_n = T_n h_n \quad (2.10)$$

where  $h_n$  is the head and  $T_n$  the transmissivity in layer  $n$ . The system simplifies to 3 uncoupled differential equations in terms of  $\phi$  (where  $\vec{\phi} = \mathbf{V}^{-1} \vec{\Phi}$ )

$$\nabla^2 \phi_n = \frac{\phi_n}{\lambda_n^2} - r_n \quad (2.11)$$

where  $r_n$  is the  $n^{\text{th}}$  element of the dot product between the inverse of the matrix  $\mathbf{V}$ , which contains the eigenvectors of matrix  $\mathbf{A}$ , and the last term in (Eq. 2.9).

$$\mathbf{V} = (\vec{e}_1 \quad \vec{e}_2 \quad \vec{e}_3) = \begin{pmatrix} e_{1,1} & e_{1,2} & e_{1,3} \\ e_{2,1} & e_{2,2} & e_{2,3} \\ e_{3,1} & e_{3,2} & e_{3,3} \end{pmatrix} \quad (2.12)$$

$$\mathbf{V}^{-1} = \begin{pmatrix} \hat{e}_{1,1} & \hat{e}_{1,2} & \hat{e}_{1,3} \\ \hat{e}_{2,1} & \hat{e}_{2,2} & \hat{e}_{2,3} \\ \hat{e}_{3,1} & \hat{e}_{3,2} & \hat{e}_{3,3} \end{pmatrix} \quad (2.13)$$

$$\vec{r} = \mathbf{V}^{-1} \begin{pmatrix} -R \\ 0 \\ 0 \end{pmatrix} \quad (2.14)$$

The solution to this differential equation can be written as

$$\phi_n = C_n \exp\left(\frac{-x}{\lambda_n}\right) + D_n \exp\left(\frac{x}{\lambda_n}\right) + r_n \lambda_n^2 \quad (2.15)$$

Six boundary conditions are needed to solve for the coefficients. The flow is zero at  $x = 0$ . In terms of  $\Phi$  this boundary condition is written as

$$\left. \frac{d\vec{\Phi}}{dx} \right|_{x=0} = \vec{0} \quad (2.16)$$

or in terms of  $\phi$ ,

$$\left. \frac{d\vec{\phi}}{dx} \right|_{x=0} = \vec{0} \quad (2.17)$$

At  $x = \frac{L}{2}$  the flow must be zero in sub-layers 2 and 3 which means that all water must flow towards the head-specified ditch in layer 1, which means all boundary conditions can be defined as a flux. However, if all the boundary conditions are fluxes there is no information about the water level in the ditch and there are an infinite number of solutions that satisfy those boundary conditions. To avoid this, the boundary condition in sub-layer 1 is defined in terms of a potential. The boundary condition in sub-layer 1 at  $x = \frac{L}{2}$  is

$$\Phi_1 \left( x = \frac{L}{2} \right) = T_1 p \quad (2.18)$$

and in sub-layers 2 and 3

$$\left. \frac{d\Phi_n}{dx} \right|_{x=\frac{L}{2}} = 0 \quad \text{for } n = 2, 3 \quad (2.19)$$

Application of the first boundary condition (Eq. 2.17) yields  $C_n = D_n$ , which allows the solution to be rewritten in terms of a hyperbolic cosine.

$$\phi_n = C_n \cosh\left(\frac{x}{\lambda_n}\right) + r_n \lambda_n^2 \quad (2.20)$$

The boundary condition in sub-layer 1 (Eq. 2.18) is not easily rewritten in terms of  $\phi$ , therefore the solution for  $\phi$  is multiplied by  $\mathbf{V}$  to get it in terms of the potential  $\Phi$ . Three equations can be defined to solve for the three unknowns:  $C_1$ ,  $C_2$  and  $C_3$ . In matrix notation

$$\begin{pmatrix} e_{1,1} \cosh\left(\frac{L}{2\lambda_1}\right) & e_{1,2} \cosh\left(\frac{L}{2\lambda_2}\right) & e_{1,3} \cosh\left(\frac{L}{2\lambda_3}\right) \\ \frac{e_{2,1}}{\lambda_1} \sinh\left(\frac{L}{2\lambda_1}\right) & \frac{e_{2,2}}{\lambda_1} \sinh\left(\frac{L}{2\lambda_2}\right) & \frac{e_{2,3}}{\lambda_1} \sinh\left(\frac{L}{2\lambda_3}\right) \\ \frac{e_{3,1}}{\lambda_1} \sinh\left(\frac{L}{2\lambda_1}\right) & \frac{e_{3,2}}{\lambda_1} \sinh\left(\frac{L}{2\lambda_2}\right) & \frac{e_{3,3}}{\lambda_1} \sinh\left(\frac{L}{2\lambda_3}\right) \end{pmatrix} \begin{pmatrix} C_1 \\ C_2 \\ C_3 \end{pmatrix} = \begin{pmatrix} pT_1 + e_{1,1}R\lambda_1^2 + e_{1,2}R\lambda_2^2 + e_{1,3}R\lambda_3^2 \\ 0 \\ 0 \end{pmatrix} \quad (2.21)$$

Solution of this system of equations yields the values of the coefficients. Denoting the matrix with  $\mathbf{Y}$  and the vector on the right-hand side with  $\vec{z}$ , the solution for the coefficient vector  $\vec{C}$  becomes

$$\vec{C} = \mathbf{Y}^{-1} \vec{z} \quad (2.22)$$

Substitution of these coefficients into the original solution for  $\phi$  (Eq. 2.20) and premultiplying by  $\mathbf{V}$  gives the potential in each layer.

$$\vec{\Phi} = \sum_{i=1}^3 \left( C_i \cosh\left(\frac{x}{\lambda_i}\right) + r_i \lambda_i^2 \right) \vec{e}_i \quad (2.23)$$

The average head in all layers is equal because all the water flowing down through the layers must also flow upwards as all water exits the system through the ditch. The average head in any sub-layer is an approximation of  $p^*$ . This approach yields a solution for the value of  $p^*$  based on the water level in the ditches, but does not lend itself to the derivation of a simple expression for  $p^*$ . Solving for the coefficients is not easily done by hand. Therefore, an alternative approach is explored.

A simpler expression for  $p^*$  is derived by expressing all the boundary conditions as fluxes. Water only enters the system through recharge with magnitude  $R \cdot L$  and exits the system through the head-specified ditches. Since the system is at steady-state, the inflow must equal the outflow. The boundary condition at  $x = \frac{L}{2}$  becomes

$$\left. \frac{d\vec{\Phi}}{dx} \right|_{x=\frac{L}{2}} = \begin{pmatrix} -\frac{RL}{2} \\ 0 \\ 0 \end{pmatrix} \quad (2.24)$$

Solving the system with the specified boundary conditions yields the following expression for the coefficients

$$C_n = \frac{a_n \lambda_n}{\sinh\left(\frac{L}{2\lambda_n}\right)} \quad (2.25)$$

with  $a_n$  equal to the  $n^{\text{th}}$  element of

$$\vec{a} = \mathbf{V}^{-1} \begin{pmatrix} -\frac{RL}{2} \\ 0 \\ 0 \end{pmatrix} \quad (2.26)$$

The complete solution for  $\phi_n$  can be written as

$$\phi_n = \frac{a_n \lambda_n \cosh\left(\frac{x}{\lambda_n}\right)}{\sinh\left(\frac{L}{2\lambda_n}\right)} + r_n \lambda_n^2 \quad (2.27)$$

This solution does not contain any information about the water level in the ditches. Since the water level at  $x = \frac{L}{2}$  is known in sub-layer 1, the solution for potential using only flux boundary conditions can be matched to the solution given by (Eq. 2.23) through a vertical translation of the solution. A constant is added so that the calculated potential at  $x = \frac{L}{2}$  is equal to the known potential in the ditch,  $pT_1$ . This constant is equal to the difference between the potential in the ditch  $pT_1$  and the calculated potential at  $x = \frac{L}{2}$ . This difference will be called  $\Delta\Phi$ . An expression for the mean potential in layer 1 is given by

$$\bar{\Phi}_1 = \sum_{i=1}^3 e_{1,i} \phi_i + \Delta\Phi \quad (2.28)$$

The relationship between the estimate for  $p^*$  and  $\bar{\Phi}_1$  is

$$p^* = \frac{\bar{\Phi}_1}{T_1} \quad (2.29)$$

The average value of the head in layer 1 between  $0 \leq x \leq \frac{L}{2}$  is the estimate for  $p^*$ . This is equivalent to integrating  $\phi_n$  between 0 and  $\frac{L}{2}$ , dividing by  $\frac{L}{2}$ , translating that result into an average potential and then calculating the average head. The calculation of the mean of  $\phi_n$  is given by

$$\begin{aligned}
\bar{\phi}_n &= \frac{2}{L} \int_0^{L/2} \frac{a_n \lambda_n \cosh\left(\frac{x}{\lambda_n}\right)}{\sinh\left(\frac{L}{2\lambda_n}\right)} - r_n \lambda_n^2 dx \\
&= \frac{2}{L} \left[ \frac{a_n \lambda_n^2 \sinh\left(\frac{x}{\lambda_n}\right)}{\sinh\left(\frac{L}{2\lambda_n}\right)} - r_n \lambda_n^2 x \right]_0^{L/2} \\
&= \frac{2}{L} \left[ a_n \lambda_n^2 - \frac{r_n \lambda_n^2 L}{2} \right] \\
&= \frac{2a_n \lambda_n^2}{L} - r_n \lambda_n^2
\end{aligned}$$

The next step is the substitution of the values for  $a_n$  and  $r_n$ . Note that  $\hat{e}_{i,j}$  is an element of the inverse of the matrix containing the eigenvectors,  $\mathbf{V}$  (see Eq. 2.13).

$$a_n = \frac{-\hat{e}_{n,1}RL}{2} \quad (2.30)$$

$$r_n = -\hat{e}_{n,1}R \quad (2.31)$$

The average value of  $\phi_n$  then is

$$\bar{\phi}_n = -\hat{e}_{n,1}R\lambda_n^2 + \hat{e}_{n,1}R\lambda_n^2 = 0$$

This result means that (Eq. 2.29) simplifies to

$$p^* = \frac{\Delta\Phi}{T_1} \quad (2.32)$$

The value of  $\Delta\Phi$  is the difference between the potential in the ditch  $pT_1$  and the value of the solution of (Eq. 2.27) in sub-layer 1 at  $x = \frac{L}{2}$ . First, the value of  $\phi_n$  at that point must be calculated.

$$\phi_n\left(x = \frac{L}{2}\right) = a_n \lambda_n \coth\left(\frac{L}{2\lambda_n}\right) - r_n \lambda_n^2 \quad (2.33)$$

Converting this result into potential  $\Phi$  and writing out the equation for  $\Delta\Phi$  yields

$$\Delta\Phi = pT_1 - \sum_{n=0}^3 e_{1,n} \hat{e}_{1,n} R \lambda_n \left( \lambda_n - \frac{L}{2} \coth\left(\frac{L}{2\lambda_n}\right) \right) \quad (2.34)$$

Writing this in terms of head to get a value for  $p^*$  gives

$$p^* = p - \frac{R}{T_1} \sum_{n=0}^3 e_{1,n} \hat{e}_{n,1} \lambda_n \left( \lambda_n - \frac{L}{2} \coth \left( \frac{L}{2\lambda_n} \right) \right) \quad (2.35)$$

This equation gives an estimate of the effective water level for a system with a phreatic layer consisting of three sub-layers. This formula can easily be generalized to work for a phreatic layer with  $N$  sub-layers where the ditch only penetrates the first sub-layer.

$$p^* = p - \frac{R}{T_1} \sum_{n=0}^N e_{1,n} \hat{e}_{n,1} \lambda_n \left( \lambda_n - \frac{L}{2} \coth \left( \frac{L}{2\lambda_n} \right) \right) \quad (2.36)$$

The formula above does not take into account the bed resistance ( $c_0$ ) of the ditches. When the value of the bed resistance is large, the flow in the subsurface will distribute itself differently. As long as the value of  $c_0$  is small (how small is discussed in Chapter 6) relative to the resistance of the aquitard, the flow in the subsurface will not be altered significantly. In those situations the approximation of an impermeable aquitard under the phreatic layer is still reasonable. To calculate the correct value for  $p^*$  the head in the phreatic layer must be increased by  $\Delta h$ , which is added to the expression for  $p^*$ . The value for  $\Delta h$  is calculated by

$$\begin{aligned} \frac{NL}{2} &= \frac{\Delta h B}{c_0} \\ \Delta h &= \frac{NLc_0}{B} \end{aligned}$$

Addition of this term accounts for the bed resistance of the ditches. It is noted that this formula only applies for small values of the bed resistance as the approximations used in the derivation for  $p^*$  are no longer valid when the value of  $c_0$  increases.

### 2.3.2 Derivation of $c^*$

The second parameter that needs to be determined is the effective resistance  $c^*$ . The conceptual model consists of three sub-layers and an aquitard at the bottom, representing the resistance layer separating the phreatic layer from the regional aquifer. The recharge is set to 0 because the recharge does not influence the value of  $c^*$ . The justification for this approximation is discussed in Chapter 6. At  $x = L/2$  there is a ditch with discharge  $Q$ . The head at the ditch is  $p_1$ . In the sub-layers below the ditch there are no-flow boundaries. At  $x = 0$  there is a water divide, which is implemented in the model as a no-flow boundary.

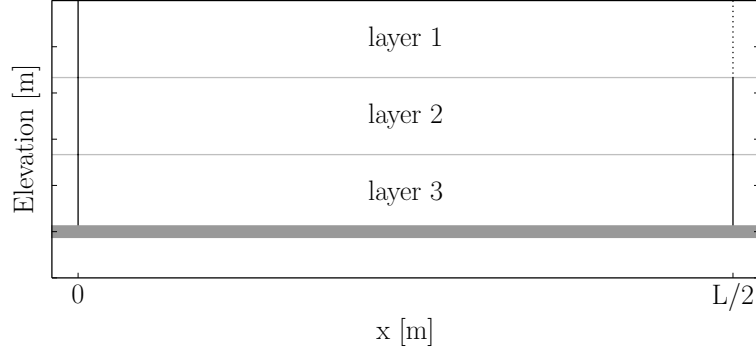


**Figure 2.5:** Conceptual model for derivation of a new formula for  $c^*$ . The dotted line in the first sub-layer is a ditch, the solid lines represent no-flow boundaries. The bottom of the model is permeable.

The total flow through the aquitard at the bottom in the detailed model must be equal to the head difference between the ditch ( $p_1$ ) and the regional aquifer ( $p_2$ ) divided by  $c^*$  multiplied by the width  $L/2$ .

$$Q = \frac{p_1 - p_2}{c^*} \frac{L}{2} \quad (2.37)$$

Parameter  $c^*$  can then be calculated by rearranging this formula

$$c^* = \frac{L(p_1 - p_2)}{2Q} \quad (2.38)$$

Since the bottom of the model is no longer impermeable, information is required about the head in the regional aquifer, denoted by  $p_2$ . This parameter is set to 0 m. This is acceptable because only the difference between the head in the ditch and the head below the resistance layer are important. (Eq. 2.38) simplifies to

$$c^* = \frac{Lp_1}{2Q} \quad (2.39)$$

The value of  $p_1$  needs to be determined. The system of differential equations describing this situation is given by the following matrix equation. Note that the system matrix is altered slightly because the bottom is no longer impermeable. A term containing the resistance of the bottom  $c_4$  is added to the last entry in the main diagonal. Previously, in the the derivation for a formula for  $p^*$  the resistance of the bottom was infinite, resulting in a value of 0 for that term.

$$\nabla^2 \vec{\Phi} \begin{pmatrix} \frac{1}{T_1 c_1} + \frac{1}{T_1 c_2} & \frac{-1}{T_2 c_2} & 0 \\ \frac{-1}{T_1 c_2} & \frac{1}{T_2 c_2} + \frac{1}{T_2 c_3} & \frac{-1}{T_3 c_3} \\ 0 & \frac{-1}{T_2 c_3} & \frac{1}{T_3 c_3} + \frac{1}{T_3 c_4} \end{pmatrix} \vec{\Phi} \quad (2.40)$$

Uncoupling this system of equations and writing it in terms of  $\phi$  yields

$$\nabla^2 \phi_n = \frac{\phi_n}{\lambda_n^2} \quad (2.41)$$

The general solution to this differential equation is well-known. Application of the boundary condition at  $x = 0$  yields the following equation

$$\phi_n = C_n \cosh\left(\frac{x}{\lambda_n}\right) \quad (2.42)$$

The solution for the constant  $C_n$  can be determined from the boundary conditions at  $x = L/2$ .

$$\frac{d\phi}{dx} = \mathbf{V}^{-1} \begin{pmatrix} Q \\ 0 \\ 0 \end{pmatrix} \quad (2.43)$$

Solving for  $C_n$  yields

$$C_n = \frac{a_n \lambda_n}{\sinh\left(\frac{L}{2\lambda_n}\right)} \quad (2.44)$$

with  $a_n$  equal to the  $n^{\text{th}}$  element of the resulting vector after matrix multiplication on the right-hand side of (Eq. 2.43).

The value of  $p_1$  can be calculated using the solution given by (Eq. 2.42) with substitution of the expression for  $C_n$  (Eq. 2.44) and  $x = L/2$ .

$$\phi_n \left(x = \frac{L}{2}\right) = a_n \lambda_n \coth\left(\frac{L}{2\lambda_n}\right) \quad (2.45)$$

Translating the result to potential

$$\Phi_n = Q \sum_{i=1}^3 e_{n,i} \hat{e}_{i,n} \lambda_i \coth\left(\frac{L}{2\lambda_i}\right) \quad (2.46)$$

The potential is divided by the transmissivity to obtain the head (the inverse of (Eq. 2.10)). The head  $p_1$  is equal to the potential in sub-layer 1 divided by the transmissivity of sub-layer 1.

$$p_1 = \frac{Q}{T_1} \sum_{i=1}^3 e_{1,i} \hat{e}_{i,1} \lambda_i \coth\left(\frac{L}{2\lambda_i}\right) \quad (2.47)$$

Substitution of this result into (Eq. 2.38) to calculate  $c^*$  gives

$$c^* = \frac{L}{2T_1} \sum_{i=1}^3 e_{1,i} \hat{e}_{i,1} \lambda_i \coth \left( \frac{L}{2\lambda_i} \right) \quad (2.48)$$

For  $N$  sub-layers in the phreatic layer the formula for  $c^*$  becomes

$$c^* = \frac{L}{2T_1} \sum_{i=1}^N e_{1,i} \hat{e}_{i,1} \lambda_i \coth \left( \frac{L}{2\lambda_i} \right) \quad (2.49)$$

This formula does not take into account the bed resistance of the ditches. Assuming flow patterns are similar with the introduction of the bed resistance, the value of  $p_1$  changes slightly. The flux from the ditch is given by

$$Q = \frac{(p_1 - p_c) B}{c_0} \frac{B}{2} \quad (2.50)$$

with  $p_c$  equal to the water level in the ditch.

$$p_1 = p_c + \frac{2Qc_0}{B} \quad (2.51)$$

When the value of the bed resistance ( $c_0$ ) is negligible the water level in the ditch is equal to the water level in the phreatic aquifer next to the ditch ( $p_1 = p_c$ ). Now, this is no longer the case and the head in the aquifer near the ditch has to be increased by the term on the right-hand side which gives

$$c^* = \frac{p_c L}{2Q} + \frac{Lc_0}{B} \quad (2.52)$$

The first term to the right of the equals sign is equal to the earlier expression for  $c^*$ . When bed resistance is not negligible the second term on the right side has to be added to the calculation of  $c^*$ . Note that this formula is only valid for small values of the bed resistance relative to the resistance of the aquitard, as larger values for  $c_0$  mean that the approximations used in this derivation are no longer valid.

### 2.3.3 Approximations

The following approximations were made in order to solve the conceptual models created to estimate the effective parameters  $p^*$  and  $c^*$ . The approximations that were also used by de Lange:

- The Dupuit-Forchheimer approximation is adopted.
- The ditches are equidistant, parallel and infinitely long.

- There is symmetry of flow.
- The groundwater recharge is constant in space and time between two ditches.

Additional approximations necessary to solve the new conceptual models.

- The transmissivity is constant in each sub-layer.
- The width of a ditch is zero. It is negligible compared to the distance between two ditches.
- In the conceptual model for the estimation of  $p^*$ , the aquitard separating the regional aquifer and the phreatic layer is impermeable.
- In the conceptual model for the estimation of  $c^*$  the recharge is set to zero. The value of the recharge has a negligible impact on the value of  $c^*$ .

## Chapter 3

# Analytic element modeling of multi-aquifer flow

The analytic element method is based on the idea that every feature observed in nature that impacts groundwater levels or flow can be represented by an analytic function. This function describes the influence of a feature on groundwater head and flow mathematically. When several features are present, the impact on groundwater at a certain point can be calculated by summing up the analytic functions of each feature. This section explains the basic theory behind analytic element modeling and derives the solutions for several different features. For more information about the analytic element method for modeling groundwater see, [Strack](#) (e.g., 2003). The object-oriented model environment based on these solutions was written in Python. Example code and a brief explanation of the program are given in [Appendix B](#).

### 3.1 Multi-layer analytic element modeling

The analytic element method is a method based on the superposition of analytic functions. Each analytic function is called an analytic element and each element corresponds to certain features observed in the real world, e.g., a ditch, a drain, an area over which infiltration takes place, etc., and describes the influence on groundwater levels and groundwater flow ([Bakker and Kelson, 2009](#)).

For steady confined Dupuit-Forchheimer flow in a homogeneous aquifer, analytic element formulations are often written in terms of a discharge potential  $\Phi$  which equals the head  $h$  multiplied by the transmissivity  $T$ . In a multi-layer approach both the head and the transmissivity become vectors containing the information of each layer ([Bakker and Strack, 2003](#)). Each element has a free parameter that defines its strength, e.g., the discharge of a ditch. The potential at a point can be calculated by superimposing the

effects of all elements at that point (Bakker and Kelson, 2009).

$$\Phi(x) = \sum_{i=1}^N p_i \Phi_i(x) \quad (3.1)$$

where  $N$  is the number of elements,  $p_i$  denotes the free parameter of element  $i$  and  $\Phi_i$  is the unit potential influence function of element  $i$ . The unit potential influence function  $\Phi_i$  is the potential of element  $i$  when its strength is set to one. In analytic element models the unit-influence function of an element is calculated first and subsequently multiplied by its strength. For some elements, such as head-specified ditches, the strength is initially unknown and must be determined from boundary conditions.

In multi-layer models the discharge potential becomes a vector  $\vec{\Phi}$  containing the discharge potential in each layer. The equation to calculate the discharge potential at a certain point then becomes

$$\vec{\Phi}(x) = \sum_{i=1}^N p_i \vec{\Phi}_i(x) \quad (3.2)$$

The discharge  $\vec{Q}_x$  of each layer is obtained from the discharge potential as

$$\vec{Q}_x = -\frac{d\vec{\Phi}(x)}{dx} \quad (3.3)$$

## 3.2 Derivation of analytic solutions for elements in a multi-layer cross-sectional model

The solutions described in this section are implemented in a cross-sectional analytic element model. Elements extend to infinity in the direction normal to the plane of flow. The head and discharge along an element does not change in the direction normal to the plane of flow.

In the next few sections, multi-layer analytic element solutions are derived for discharge-specified ditches, head-specified ditches, ditches with a bed resistance, no-flow elements, and areal recharge, based on the solution method presented by Hemker (1984).

### 3.2.1 Setting up and solving the differential equation without areal recharge

Consider a multi-layer system with  $N$  aquifers and  $N$  leaky layers. Leaky layer  $n$  is above aquifer  $n$ . The bottom of the system is impermeable (see Figure 3.1). Areal recharge is zero (the situation with non-zero areal recharge is solved in Section 3.2.6). The differential equation for flow in aquifer  $n$

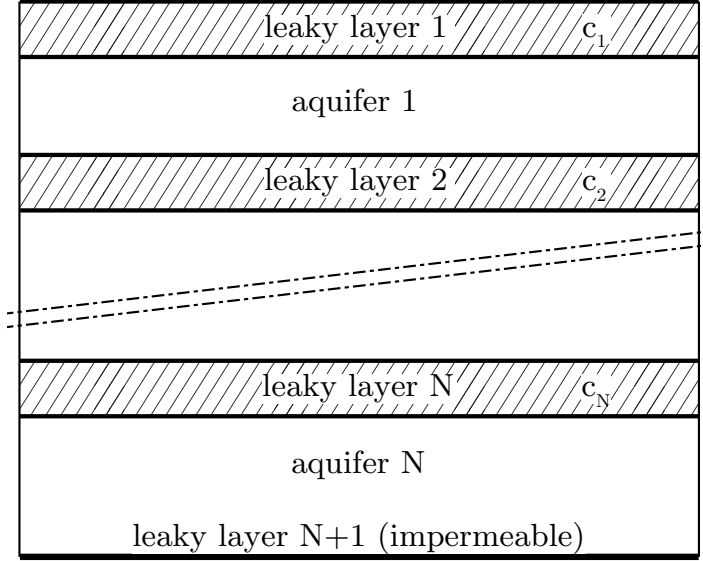


**Figure 3.1:** Aquifer system definition.

follows from a mass balance and Darcy's Law as

$$\frac{d^2 h_n}{dx^2} = \frac{h_n - h_{n-1}}{c_n T_n} + \frac{h_n - h_{n+1}}{c_{n+1} T_n} \quad n = 1, \dots, N - 1 \quad (3.4)$$

and the equation for layer  $N$  is given by

$$\frac{d^2 h_N}{dx^2} = \frac{h_N - h_{N-1}}{c_N T_N} \quad (3.5)$$

where  $h$  equals the head,  $T$  the transmissivity, and  $c$  the resistance of the leaky layer. Note that the head in layer 0,  $h_0$ , is set to 0. Equations (3.4) and (3.5) can be rewritten in terms of a discharge potential  $\Phi (= Th)$  as

$$\frac{d^2 \Phi_n}{dx^2} = \frac{\Phi_n}{c_n T_n} - \frac{\Phi_{n-1}}{c_n T_{n-1}} + \frac{\Phi_n}{c_{n+1} T_n} - \frac{\Phi_{n+1}}{c_{n+1} T_{n+1}} \quad (3.6)$$

$$\frac{d^2 \Phi_N}{dx^2} = \frac{\Phi_N}{c_N T_N} - \frac{\Phi_{N-1}}{c_N T_{N-1}} \quad (3.7)$$

This system of coupled differential equations can be written in matrix form as

$$\nabla^2 \begin{pmatrix} \Phi_1 \\ \Phi_2 \\ \vdots \\ \Phi_{N-1} \\ \Phi_N \end{pmatrix} = \begin{pmatrix} \frac{1}{c_1 T_1} + \frac{1}{c_2 T_1} & \frac{-1}{c_2 T_2} & & & & \\ & \frac{-1}{c_2 T_1} & \frac{1}{c_2 T_2} + \frac{1}{c_3 T_2} & \frac{-1}{c_3 T_3} & & \\ & & \ddots & \ddots & \ddots & \\ & & & \frac{-1}{c_{N-1} T_{N-2}} & \frac{1}{c_{N-1} T_{N-1}} + \frac{1}{c_N T_{N-1}} & \frac{-1}{c_N T_N} \\ & & & & \frac{-1}{c_N T_{N-1}} & \frac{1}{c_N T_N} \end{pmatrix} \begin{pmatrix} \Phi_1 \\ \Phi_2 \\ \vdots \\ \Phi_{N-1} \\ \Phi_N \end{pmatrix} \quad (3.8)$$

The matrix equation above can be written symbolically as

$$\nabla^2 \vec{\Phi} = \mathbf{A} \vec{\Phi} \quad (3.9)$$

where  $\mathbf{A}$  is an  $N$  by  $N$  matrix with  $N$  positive eigenvalues  $\omega_n$  and corresponding eigenvectors  $\vec{e}_n$ . The relation between a matrix  $\mathbf{A}$  and its eigenvalues and eigenvectors is given by

$$\mathbf{A} \mathbf{V} = \mathbf{V} \mathbf{W} \quad (3.10)$$

where  $\mathbf{V}$  is a matrix with eigenvector  $\vec{e}_n$  in column  $n$  and  $\mathbf{W}$  is a matrix with the eigenvalues of  $\mathbf{A}$  on its diagonal. Right multiplication of both sides with  $\mathbf{V}^{-1}$  gives

$$\mathbf{A} = \mathbf{V} \mathbf{W} \mathbf{V}^{-1} \quad (3.11)$$

Using equation (3.11) to substitute for  $\mathbf{A}$  in equation 3.9 yields

$$\nabla^2 \vec{\Phi} = \mathbf{V} \mathbf{W} \mathbf{V}^{-1} \vec{\Phi} \quad (3.12)$$

Left multiplication of both sides with  $\mathbf{V}^{-1}$  and introducing a new vector  $\vec{\phi}$

$$\vec{\phi} = \mathbf{V}^{-1} \vec{\Phi} \quad (3.13)$$

gives

$$\nabla^2 \vec{\phi} = \mathbf{W} \vec{\phi} \quad (3.14)$$

This matrix equation is a set of  $N$  uncoupled differential equations

$$\begin{aligned} \nabla^2 \phi_1 &= \omega_1 \phi_1 \\ \nabla^2 \phi_2 &= \omega_2 \phi_2 \\ &\vdots \\ \nabla^2 \phi_N &= \omega_N \phi_N \end{aligned} \quad (3.15)$$

The eigenvalues are often replaced by so-called leakage factors  $\lambda$  defined as

$$\lambda = \frac{1}{\sqrt{\omega}} \quad (3.16)$$

Substitution of  $\lambda$  for  $\omega$  gives

$$\nabla^2 \phi_i = \frac{\phi_i}{\lambda_i^2} \quad \text{for } i = 1, \dots, N \quad (3.17)$$

which is known as the modified Helmholtz equation. The general solution to this differential equation (3.17) is

$$\phi_i = C_i \exp\left(\frac{-x}{\lambda_i}\right) + D_i \exp\left(\frac{x}{\lambda_i}\right) \quad \text{for } i = 1, \dots, N \quad (3.18)$$

where  $C_i$  and  $D_i$  are arbitrary constants. The derivative of  $\phi$  is given by

$$\frac{d\phi_i}{dx} = -\frac{C_i}{\lambda} \exp\left(\frac{-x}{\lambda_i}\right) + \frac{D_i}{\lambda} \exp\left(\frac{x}{\lambda_i}\right) \quad \text{for } i = 1, \dots, N \quad (3.19)$$

Once a solution for  $\phi_i$  has been found, the solution for the potential vector  $\vec{\Phi}$  is obtained by taking the inverse of (Eq. 3.13).

$$\vec{\Phi} = \mathbf{V}\vec{\phi} = \phi_1 \vec{e}_1 + \phi_2 \vec{e}_2 + \dots + \phi_N \vec{e}_N \quad (3.20)$$

The values of the coefficients  $C_i$  and  $D_i$  for  $i = 1, \dots, N$  depend on the boundary conditions. The solutions for different boundary conditions are presented in the next sections.

### 3.2.2 Ditch element with given discharge

A ditch with a given discharge is the most basic type of element. There are no unknown parameters. The coefficients in the general solution (Eq. 3.18) may be determined from boundary conditions and the head or discharge can be calculated at any point along the cross-section. The solution is derived using an example. Note that magnitude of the discharge of an element is also referred to as its strength.

Consider the following situation: a ditch is located at  $x = 0$  in a multi-aquifer model, with given discharge  $Q$ . First, only the region where  $x \geq 0$  is considered. The solution for  $\Phi$  must be bounded in the interval  $(0, \infty)$ ; the potential cannot go to infinity when  $x \rightarrow \infty$ , therefore coefficient  $D$  must equal zero. That leaves a single coefficient to be determined. The boundary condition at  $x = 0$  is

$$\vec{Q}_x = -\frac{d\vec{\Phi}}{dx} = -\frac{\vec{q}}{2} \quad (3.21)$$

where  $\vec{q}$  is a vector containing the discharge  $q_i$  of the ditch in each layer. Note that  $q_i$  is divided by two because only the region  $x \geq 0$  is considered.

The assumption is that half the total discharge flows in from one side. The other half of the discharge comes from the region  $x < 0$ . Substitution of (Eq. 3.20) in (Eq. 3.21) gives

$$\mathbf{V} \frac{d\vec{\phi}}{dx} = \frac{\vec{q}}{2} \quad (3.22)$$

Substitution of (Eq. 3.19) for the components of  $\frac{d\vec{\phi}}{dx}$  and zero for  $x$  gives

$$\begin{pmatrix} e_{1,1} & e_{1,2} & e_{1,3} \\ e_{2,1} & e_{2,2} & e_{2,3} \\ e_{3,1} & e_{3,2} & e_{3,3} \end{pmatrix} \begin{pmatrix} \frac{C_1}{\lambda_1} \\ \frac{C_2}{\lambda_2} \\ \vdots \\ \frac{C_N}{\lambda_N} \end{pmatrix} = \begin{pmatrix} \frac{q_1}{2} \\ \frac{q_2}{2} \\ \vdots \\ \frac{q_N}{2} \end{pmatrix} \quad (3.23)$$

The coefficients  $\vec{C}$  may now be obtained as

$$\vec{C} = (\mathbf{V}^{-1}\vec{q}) \odot \vec{\lambda} \quad (3.24)$$

where the matrix product of  $\mathbf{V}^{-1}$  and  $\vec{q}$  has to be multiplied elementwise (denoted by the  $\odot$  symbol) with a vector containing  $\lambda_1, \dots, \lambda_N$  to calculate  $C_1, \dots, C_N$ .

The unit potential influence of an element (the potential of the element if its strength were set to 1) is calculated by setting  $\vec{q}$  to minus one for the layer in which the element is located. The negative sign indicates that a ditch with a positive discharge pumps water out of the system.

The final solution for the potential, adding in the coordinate of the ditch  $x_c$  (in case  $x_c \neq 0$ ), becomes

$$\vec{\Phi} = \begin{cases} \sum_{i=1}^N C_i \exp\left(\frac{-(x-x_c)}{\lambda_i}\right) \vec{v}_i & \text{for } x - x_c \geq 0 \\ \sum_{i=1}^N C_i \exp\left(\frac{(x-x_c)}{\lambda_i}\right) \vec{v}_i & \text{for } x - x_c < 0 \end{cases} \quad (3.25)$$

The potential vector  $\vec{\Phi}$  has to be divided elementwise by the transmissivity  $\vec{T}$  for each layer to calculate the head. The solution for the discharge in each layer follows from (Eq. 3.3)

$$\vec{Q}_x = \begin{cases} \sum_{i=1}^N \frac{C_i}{\lambda_i} \exp\left(\frac{-(x-x_c)}{\lambda_i}\right) \vec{v}_i & \text{for } x - x_c \geq 0 \\ \sum_{i=1}^N -\frac{C_i}{\lambda_i} \exp\left(\frac{(x-x_c)}{\lambda_i}\right) \vec{v}_i & \text{for } x - x_c < 0 \end{cases} \quad (3.26)$$

### 3.2.3 Ditch element with given head

A ditch element with given head is very similar to a ditch element with given discharge. The strength,  $q$ , is now an unknown that has to be determined from the specified head. The solution is described using a simple example (for another example, see e.g. Bakker and Kelson (2009)).

Recall from Section 3.2 that the strength  $q$  is the free parameter for a ditch element in an analytic element model. The potential can be written as

$$\Phi^* = q_i \Phi_i(x) \quad (3.27)$$

where  $\Phi_i$  is the unit potential influence of element  $i$ . If there are several elements, the potentials of all elements are added together (Eq. 3.2).

Consider a two-layer model with three ditches in the top aquifer. The first two ditches are head-specified ditches and the last one is discharge specified. The coordinates of the ditches are  $x_1$ ,  $x_2$ , and  $x_3$  respectively. For the two head-specified ditches the value for the potential at  $x_1$  and  $x_2$  is known.

$$\begin{aligned} \text{At } x = x_1 : \quad h = h_1 \quad \text{and} \quad \Phi_1^* = h_1 T_1 \\ \text{At } x = x_2 : \quad h = h_2 \quad \text{and} \quad \Phi_2^* = h_2 T_1 \end{aligned}$$

Using this information and (Eq. 3.2) two equations can be defined

$$\begin{aligned} \Phi_1^* &= q_1 \Phi_{1,1}(x = x_1) + q_2 \Phi_{2,1}(x = x_1) + q_3 \Phi_{3,1}(x = x_1) \\ \Phi_2^* &= q_1 \Phi_{1,1}(x = x_2) + q_2 \Phi_{2,1}(x = x_2) + q_3 \Phi_{3,1}(x = x_2) \end{aligned}$$

where  $\Phi_{i,j}(x)$  indicates the unit potential of element  $i$  in layer  $j$  at point  $x$ .  $q_1$  and  $q_2$  are the unknowns that need to be determined. Since  $q_3$  is known it can be subtracted from both sides. Rewriting in matrix form then gives

$$\begin{pmatrix} \Phi_{1,1}(x = x_1) & \Phi_{2,1}(x = x_1) \\ \Phi_{1,1}(x = x_2) & \Phi_{2,1}(x = x_2) \end{pmatrix} \begin{pmatrix} q_1 \\ q_2 \end{pmatrix} = \begin{pmatrix} \Phi_1^* - q_3 \Phi_{3,1}(x = x_1) \\ \Phi_2^* - q_3 \Phi_{3,1}(x = x_2) \end{pmatrix} \quad (3.28)$$

This system can easily be solved for  $q_1$  and  $q_2$  which can then be used with (Eq. 3.25 and 3.26) to calculate the potential and discharge. When there is more than one element (Eq. 3.2) is used to calculate the total potential at any point in the cross-section.

### 3.2.4 Head-specified ditch element with bed resistance

In ditches or rivers there is generally a resistance to the in- or out-flow of water caused by the deposition of fine sediments and organic material. This resistance can be schematized by a thin resistance layer with a resistance

$c_0$  at the bottom of the canal. The flux to a ditch from the aquifer can be written as the ratio between the head difference and the resistance  $c_0$  multiplied by the wet circumference of the ditch  $w$  (which is equal to the width of a ditch for shallow ditches).

$$q = \frac{h - p}{c_0} w \quad (3.29)$$

where  $h$  is the head in the aquifer and  $p$  is the water level in the ditch. Equation (3.29) is rewritten to obtain an expression for  $h$ .

$$h = \frac{q}{C_c} + p \quad (3.30)$$

where parameter  $C_c = w/c_0$  is also known as the ditch conductance. The previous equation can also be written in terms of potential  $\Phi$  by multiplying both sides with transmissivity  $T$

$$\Phi = \frac{qT}{C_c} + Tp \quad (3.31)$$

The example from the previous section with three ditches in the top aquifer is revisited to show how parameter  $q$  is determined. The ditches at  $x = x_1$  and  $x = x_2$  are ditches with a bed resistance  $c_0$  and width  $w$ . The third ditch at  $x = x_3$  remains a discharge-specified ditch.

$$\begin{aligned} \text{At } x = x_1 : \quad h &= \frac{q_1}{C_c} + p \quad \text{and} \quad \Phi_1^* = \frac{q_1 T_1}{C_c} + T_1 p \\ \text{At } x = x_2 : \quad h &= \frac{q_2}{C_c} + p \quad \text{and} \quad \Phi_2^* = \frac{q_2 T_1}{C_c} + T_1 p \end{aligned} \quad (3.32)$$

The potential in the aquifer at  $x = x_i$  can also be written as

$$\Phi_i^* = q_1 \Phi_{1,1}(x = x_i) + q_2 \Phi_{2,1}(x = x_i) + q_3 \Phi_{3,1}(x = x_i) \quad \text{for } i = 1, 2 \quad (3.33)$$

Substitution of (Eq. 3.32) in (Eq. 3.33) and rearranging yields

$$q_1 \left( \Phi_{1,1}(x = x_1) - \frac{T_1}{C_c} \right) + q_2 \Phi_{2,1}(x = x_1) = T_1 p - q_3 \Phi_{3,1}(x = x_1) \quad (3.34)$$

$$q_1 \Phi_{1,1}(x = x_2) + q_2 \left( \Phi_{2,1}(x = x_2) - \frac{T_1}{C_c} \right) = T_1 p - q_3 \Phi_{3,1}(x = x_2) \quad (3.35)$$

which can be written in matrix notation as

$$\begin{pmatrix} \Phi_{1,1}(x = x_1) - \frac{T_1}{C_c} & \Phi_{2,1}(x = x_1) \\ \Phi_{1,1}(x = x_2) & \Phi_{2,1}(x = x_2) - \frac{T_1}{C_c} \end{pmatrix} \begin{pmatrix} q_1 \\ q_2 \end{pmatrix} = \begin{pmatrix} T_1 p - q_3 \Phi_{3,1}(x = x_1) \\ T_1 p - q_3 \Phi_{3,1}(x = x_2) \end{pmatrix} \quad (3.36)$$

Solving this system of equations for  $\vec{q}$  allows the head or discharge to be calculated at any point in the cross-section.

### 3.2.5 No-flow boundary element

The no-flow boundary element is a special case of the basic ditch element. The strength is determined by requiring the flow to be zero at a point near the element. There are two versions of this element, where this point lies either to the left or right of the element. When this one-sided element is included in the model, the region beyond these boundaries is no longer considered. The no-flow condition is given by the following formula

$$\Psi \vec{q} = \vec{0} \quad (3.37)$$

where  $\Psi$  is a matrix with the unit discharge influence of each element at the location of an element with an unknown free parameter in each row. Recall that the unit discharge influence is the influence of an element on the total discharge at a specific point when its strength is set to one.

Consider the example from the previous sections. The elements at  $x = x_1$  and  $x_2$  are now converted to no-flow boundary elements. The discharge-specified canal at  $x = x_3$  lies between the two boundary elements ( $x_1 < x_3 < x_2$ ). The discharge at a small distance,  $\Delta x$ , to the right of  $x_1$  must equal zero. The value of  $\Delta x$  is, e.g.,  $10^{-6}$  m.

$$Q_x(x_1 + \Delta x) = q_1 \Psi_{1,1}(x_1 + \Delta x) + q_2 \Psi_{2,1}(x_1 + \Delta x) + q_3 \Psi_{3,1}(x_1 + \Delta x) = 0 \quad (3.38)$$

At the right no-flow boundary  $\Delta x$  is subtracted from  $x_2$ .

$$Q_x(x_2 - \Delta x) = q_1 \Psi_{1,1}(x_2 - \Delta x) + q_2 \Psi_{2,1}(x_2 - \Delta x) + q_3 \Psi_{3,1}(x_2 - \Delta x) = 0 \quad (3.39)$$

In matrix notation this becomes

$$\begin{pmatrix} \Psi_{1,1}(x_1 + \Delta x) & \Psi_{2,1}(x_1 + \Delta x) \\ \Psi_{1,1}(x_2 - \Delta x) & \Psi_{2,1}(x_2 - \Delta x) \end{pmatrix} \begin{pmatrix} q_1 \\ q_2 \end{pmatrix} = \begin{pmatrix} -q_3 \Psi_{3,1}(x_1 + \Delta x) \\ -q_3 \Psi_{3,1}(x_2 - \Delta x) \end{pmatrix} \quad (3.40)$$

Once the solution for  $\vec{q}$  is obtained the head and discharge can be calculated at any point in the cross-section between the no-flow boundaries.

### 3.2.6 Areal infiltration

Adding recharge to a groundwater model alters the governing differential equation for the region in which there is recharge by adding a flux  $R$  at the top of the first layer. The general differential equation then becomes

$$\nabla^2 \vec{\Phi} = \mathbf{A} \vec{\Phi} + \vec{R} \quad (3.41)$$

where  $\vec{R}$  is equal to

$$\vec{R} = \begin{pmatrix} -R \\ 0 \\ \vdots \\ 0 \\ 0 \end{pmatrix} \quad (3.42)$$

$R$  is the amount of water that infiltrates into the top layer in meters per day.  $R$  is zero in all but the first layer of the model as recharge only occurs in the topmost layer. The negative sign ensures that a positive value for the recharge puts water into the system. When the unit potential influence needs to be calculated  $-R$  is replaced by  $-1$ .

Substitution of (Eq. 3.11) for  $\mathbf{A}$  and introducing the vector  $\vec{\phi} = \mathbf{V}^{-1}\vec{\Phi}$  we get the following system of uncoupled differential equations

$$\nabla^2 \vec{\phi} = \mathbf{W}\vec{\phi} + \mathbf{V}^{-1}\vec{R} \quad (3.43)$$

The  $n^{\text{th}}$  uncoupled differential equation is

$$\nabla^2 \phi_n = \frac{\phi_n}{\lambda_n^2} - a_n \quad (3.44)$$

where  $\lambda$  is defined by (Eq. 3.16). The value  $a_n$  is the  $n^{\text{th}}$  element of the vector  $\vec{a} = \mathbf{V}^{-1}\vec{R}$ . The solution to this differential equation has the following form

$$\phi_n = A_n \exp\left(\frac{-x}{\lambda_n}\right) + B_n \exp\left(\frac{x}{\lambda_n}\right) + a_n \lambda_n^2 \quad (3.45)$$

Outside the region in which areal infiltration is defined the general solution is given by (Eq. 3.18). For the solutions outside the domain in which areal infiltration has been defined, one term must equal zero for the solution to remain bounded as  $x \rightarrow \pm\infty$ . The following system of equations describes the solution. The variable  $x_c$  denotes the central coordinate of the areal infiltration element with length  $2L$ .

$$\phi_n = \begin{cases} A_n \exp\left(\frac{-(x-x_c)}{\lambda_n}\right) + B_n \exp\left(\frac{x-x_c}{\lambda_n}\right) + a_n \lambda_n^2 & \text{for } -L \leq x - x_c \leq L \\ C_n \exp\left(\frac{-(x-x_c-L)}{\lambda_n}\right) & \text{for } x - x_c \geq L \\ D_n \exp\left(\frac{x-x_c+L}{\lambda_n}\right) & \text{for } x - x_c \leq -L \end{cases} \quad (3.46)$$

Boundary conditions are defined to solve for the coefficients  $A_n$ ,  $B_n$ ,  $C_n$ , and  $D_n$  for  $n = 1, \dots, N$ . For the calculation of the constants a single aquifer is considered. Due to symmetry there is a water divide at  $x = x_c$ , the midpoint of the areal infiltration element. Symmetry means that  $A_n = B_n$  and  $C_n = D_n$ . Across the edges of the infiltration area the head (or potential) and the discharge must be continuous, resulting in the following set of conditions

1. At  $x = x_c$   $\vec{Q}_x = 0$
2. At  $x = x_c + L$   $\vec{\Phi}_{\text{left}} = \vec{\Phi}_{\text{right}}$

3. At  $x = x_c + L$   $\vec{Q}_{x,\text{left}} = \vec{Q}_{x,\text{right}}$

The first boundary condition allows simplification of (Eq. 3.46), which yields

$$\phi_n = \begin{cases} A_n \cosh\left(\frac{(x-x_c)}{\lambda_n}\right) + a_n \lambda_n^2 & \text{for } -L \leq x - x_c \leq L \\ C_n \exp\left(\frac{-(x-x_c-L)}{\lambda_n}\right) & \text{for } x - x_c \geq L \\ C_n \exp\left(\frac{x-x_c+L}{\lambda_n}\right) & \text{for } x - x_c \leq -L \end{cases} \quad (3.47)$$

The third boundary condition is written in terms of a discharge, which can be translated to a condition in terms of  $\vec{\phi}$  using (Eq. 3.20).

$$\begin{aligned} \vec{Q}_{x,\text{left}} &= \vec{Q}_{x,\text{right}} \\ -\frac{d\vec{\Phi}_{\text{left}}}{dx} &= -\frac{d\vec{\Phi}_{\text{right}}}{dx} \\ \frac{d\mathbf{V}\vec{\phi}_{\text{left}}}{dx} &= \frac{d\mathbf{V}\vec{\phi}_{\text{right}}}{dx} \end{aligned}$$

which, because  $\mathbf{V}$  is constant, is equal to

$$\frac{d\vec{\phi}_{\text{left}}}{dx} = \frac{d\vec{\phi}_{\text{right}}}{dx}$$

The derivative of  $\phi_n$  is given by

$$\frac{d\phi_n}{dx} = \begin{cases} \frac{A_n}{\lambda_n} \sinh\left(\frac{x-x_c}{\lambda_n}\right) & \text{for } -L \leq x - x_c \leq L \\ -\frac{C_n}{\lambda_n} \exp\left(\frac{-(x-x_c-L)}{\lambda_n}\right) & \text{for } x - x_c \geq L \\ \frac{C_n}{\lambda_n} \exp\left(\frac{x-x_c+L}{\lambda_n}\right) & \text{for } x - x_c \leq -L \end{cases} \quad (3.48)$$

With  $x = x_c + L$  the third boundary condition can be written as

$$\frac{A_n}{\lambda_n} \sinh\left(\frac{L}{\lambda_n}\right) = -\frac{C_n}{\lambda_n} \quad (3.49)$$

which means

$$C_n = -A_n \sinh\left(\frac{L}{\lambda_n}\right) \quad (3.50)$$

The second boundary condition is written in terms of a potential which is translated into a condition in terms of  $\vec{\phi}$ .

$$\begin{aligned} \vec{\Phi}_{\text{left}} &= \vec{\Phi}_{\text{right}} \\ \mathbf{V}\vec{\phi}_{\text{left}} &= \mathbf{V}\vec{\phi}_{\text{right}} \\ \vec{\phi}_{\text{left}} &= \vec{\phi}_{\text{right}} \end{aligned}$$

Substitution of (Eq. 3.50) with  $x = x_c + L$  gives

$$A_n \cosh\left(\frac{L}{\lambda_n}\right) + a_n \lambda_n^2 = -A_n \sinh\left(\frac{L}{\lambda_n}\right) \quad (3.51)$$

which yields

$$A_n = \frac{-a_n \lambda_n^2}{\exp\left(\frac{L}{\lambda_n}\right)} \quad (3.52)$$

Substitution of (Eq. 3.52) in (Eq. 3.50) gives

$$C_n = a_n \lambda_n^2 \left(1 - \exp\left(\frac{-2L}{\lambda_n}\right)\right) \quad (3.53)$$

After some algebra this results in the following solution for  $\phi$

$$\phi_n = \begin{cases} a_n \lambda_n^2 \left(1 - \frac{\cosh\left(\frac{x-x_c}{\lambda_n}\right)}{\exp\left(\frac{L}{\lambda_n}\right)}\right) & \text{for } -L \leq x \leq L \\ a_n \lambda_n^2 \left[\exp\left(\frac{-(x-x_c-L)}{\lambda_n}\right) - \exp\left(\frac{-(x-x_c+L)}{\lambda_n}\right)\right] & \text{for } x \geq L \\ a_n \lambda_n^2 \left[\exp\left(\frac{x-x_c+L}{\lambda_n}\right) - \exp\left(\frac{x-x_c-L}{\lambda_n}\right)\right] & \text{for } x \leq -L \end{cases} \quad (3.54)$$

This is the solution for  $\phi_n$  with the infiltration area centered around  $x_c$ . The solution in terms of a potential in layer  $n$  is found by doing the inverse of (Eq. 3.20).

$$\Phi_n = \begin{cases} \sum_{i=1}^N \epsilon_{n,i} a_i \lambda_i^2 \left(1 - \frac{\cosh\left(\frac{x-x_c}{\lambda_i}\right)}{\exp\left(\frac{L}{\lambda_i}\right)}\right) & \text{for } -L \leq x - x_c \leq L \\ \sum_{i=1}^N \epsilon_{n,i} a_i \lambda_i^2 \left[\exp\left(\frac{-(x-x_c-L)}{\lambda_i}\right) - \exp\left(\frac{-(x-x_c+L)}{\lambda_i}\right)\right] & \text{for } x - x_c \geq L \\ \sum_{i=1}^N \epsilon_{n,i} a_i \lambda_i^2 \left[\exp\left(\frac{x-x_c+L}{\lambda_i}\right) - \exp\left(\frac{x-x_c-L}{\lambda_i}\right)\right] \vec{v}_i & \text{for } x - x_c \leq -L \end{cases} \quad (3.55)$$

Generalizing the resulting formulas yields an expression for the head in accordance with (Eq. 19 and 20) in Hunt (1986). The discharge in layer  $n$  is calculated by taking the derivative of (Eq. 3.55) and multiplying by  $-1$ .

$$Q_{x,n} = \begin{cases} \sum_{i=1}^N \frac{\epsilon_{n,i} a_i \lambda_i \sinh\left(\frac{x-x_c}{\lambda_i}\right)}{\exp\left(\frac{L}{\lambda_i}\right)} & \text{for } -L \leq x - x_c \leq L \\ \sum_{i=1}^N \epsilon_{n,i} a_i \lambda_i \left[\exp\left(\frac{-(x-x_c-L)}{\lambda_i}\right) - \exp\left(\frac{-(x-x_c+L)}{\lambda_i}\right)\right] & \text{for } x - x_c > L \\ -\sum_{i=1}^N \epsilon_{n,i} a_i \lambda_i \left[\exp\left(\frac{x-x_c+L}{\lambda_i}\right) - \exp\left(\frac{x-x_c-L}{\lambda_i}\right)\right] & \text{for } x - x_c < -L \end{cases} \quad (3.56)$$

## Chapter 4

# Comparison of upscaling methods for homogeneous phreatic layers

This chapter presents the results of the comparison between upscaled models using the two upscaling methods and the explicit model in homogeneous phreatic layers. First, the streamlines for a homogeneous phreatic layer are examined to gain insight into the flow-pattern in the top system. In Section 4.2 the set-up of the models is described. The performance of the upscaling methods is presented in Section 4.3. The chapter ends with a discussion.

### 4.1 Flow through homogeneous phreatic layers

The flow in an isotropic homogeneous phreatic layer is examined in a model containing all features explicitly. The geology of this model is described in the next section. Figure 4.1 shows streamlines in the phreatic layer between several ditches in a clayey phreatic layer with recharge and partially penetrating ditches. The streamlines show the distribution of infiltrated water to the ditches and the regional aquifer. The impact of the partial penetration of the ditches is apparent; the streamlines converge close to the ditches, increasing the resistance to flow. This effect is captured by the addition of radial resistance in de Lange's upscaling method. In the multi-layer upscaling method this effect is taken into account by subdividing the phreatic layer into a number of sub-layers.

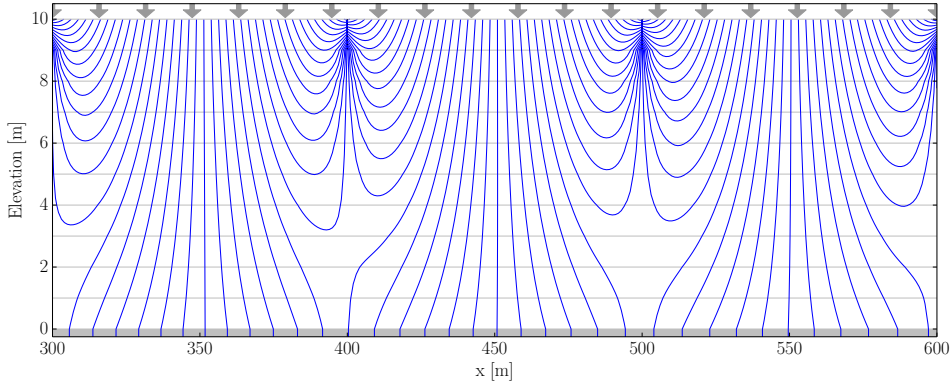


**Figure 4.1:** Streamlines for a clayey homogeneous phreatic layer (the vertical dimension is exaggerated  $10\times$ ).

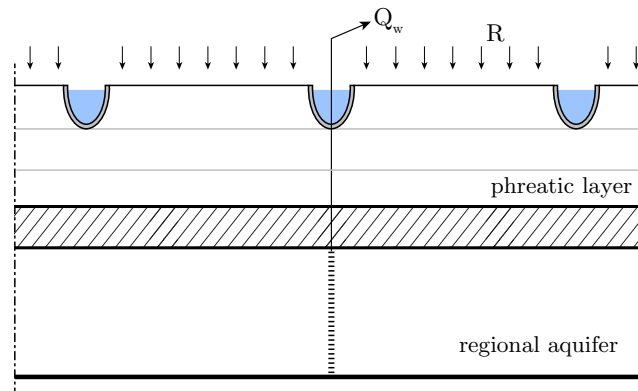
## 4.2 Description of model set-up

The two upscaling methods described in Chapter 2 are used to create up-scaled models that are compared to the analytic element model that simulates the ditches and layering of the phreatic layer explicitly. A drain (a reasonable approximation of a row of wells) is placed in the regional aquifer with a pumping rate  $Q_w$  in  $\text{m}^2/\text{d}$ . The drain is located halfway between two ditches. The number of ditches included in the explicit model is chosen such that the discharge at the model edge is less than 1% of the extraction rate. The upscaling methods are applied to replace the top-system in Figure 4.2a with a linear head-flux relationship as seen in Figure 4.2b. The upscaled model with de Lange’s parameters is denoted by  $M_{\text{DL}}$ , the upscaled model with multi-layer parameters is denoted by  $M_{\text{ML}}$ , and the analytic element model is denoted by  $M_{\text{exp}}$ . The head and the drawdown in the regional aquifer are compared for different configurations of the phreatic layer.

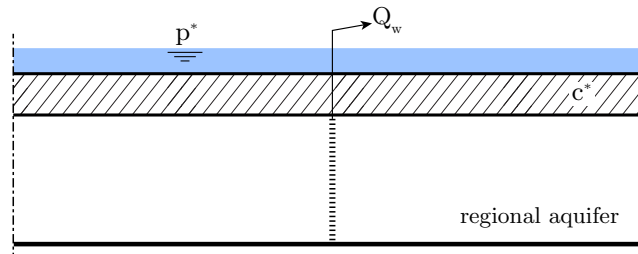
**Table 4.1:** Parameter values describing the subsurface and layout of ditches in the explicit model (see Figure 4.3).

Parameter	Values	Units	Parameter	Values	Units
$c_0$	0	d	$c_1$	1000	d
$k_{\text{phreatic}}$	1.0	m/d	$k_{\text{regional}}$	25	m/d
$L$	100	m	$p$	9.0	m
$H_{\text{phreatic}}$	10	m	$H_{\text{regional}}$	40	m
$N$	0.001	m/d	$Q_w$	0.1, 1.0, 10.0	$\text{m}^2/\text{d}$

Figure 4.3 shows the relevant physical characteristics of the explicit model. The magnitude of these parameters is presented in Table 4.1. The phreatic layer in the explicit model has a thickness of  $H_{\text{phreatic}} = 10$  meters.



(a) Explicit model



(b) Upscaled model

**Figure 4.2:** Conceptualizations of the explicit model (a) and the upscaled model (b) with a drain in the regional aquifer with pumping rate  $Q_w$ .

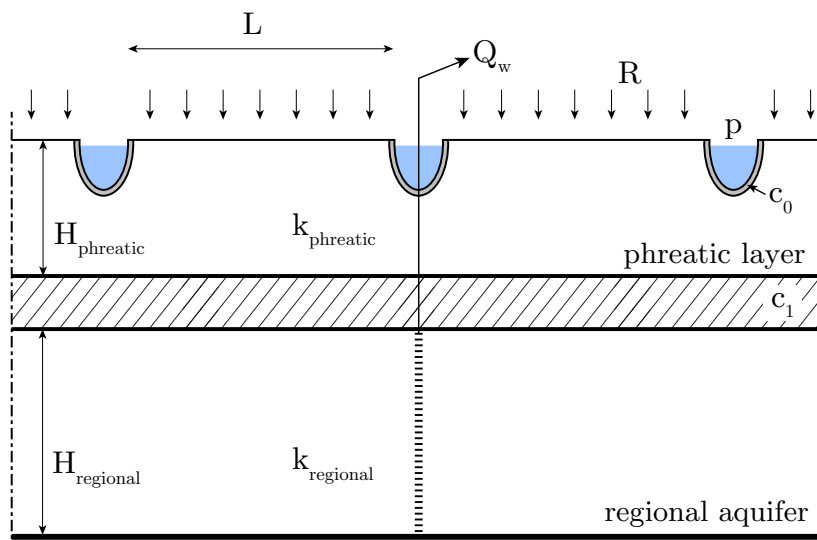


**Figure 4.3:** Conceptual model of the subsurface.

The aquitard has a thickness of 5 meters and a resistance of  $c_1 = 1000$  days. The regional aquifer is  $H_{regional} = 40$  meters thick. The recharge is set to  $R = 1$  millimeter per day. The water level in the ditches is  $p = 9.0$  meters above reference level (the top of the aquitard). The bed resistance of the ditches is set to  $c_0 = 0$  ( $10^{-5}$  d in the model). The ditches are uniformly spaced with distance  $L = 100$  m. The width of the ditches is negligible compared to the distance between them.

### 4.3 Performance of upscaling methods

Three scenarios with different configurations of the homogeneous phreatic layer are considered (Table 4.2). The horizontal hydraulic conductivity is equal in each sub-layer and is set to 1 m/d, representing a permeable clay. Scenario 1 is a single-layer with fully penetrating canals, which is closely related to the conceptual model from which [de Lange \(1999\)](#) derived his formulas. In Scenario 2, the ditches partially penetrate the phreatic layer. In Scenario 3, strong vertical anisotropy is introduced; the vertical hydraulic conductivity is one-tenth the value of the horizontal hydraulic conductivity.

**Table 4.2:** Description of the schematization of the phreatic layer for the explicit model. The upscaled models are tested against the explicit model for each scenario.

Scenario	Phreatic layer characteristics
1	Homogeneous phreatic layer consisting of a single layer. Ditches are fully penetrating, conductivity is isotropic
2	Homogeneous phreatic layer consisting of 10 sub-layers. Ditches partially penetrate the phreatic layer, conductivity is isotropic
3	Homogeneous phreatic layer consisting of 10 sub-layers. Ditches partially penetrate the phreatic layer, conductivity is anisotropic

Two comparisons are performed to assess the performance of the two upscaling methods. The drawdown in the regional aquifer in the upscaled models is compared to the drawdown in the explicit model. The drawdown is calculated by subtracting the head calculated by the model from the groundwater level at a large distance from the drain. The performance is expressed as the quotient of the drawdown in the upscaled model divided by the drawdown in the explicit model. Since drawdown is linearly related to the magnitude of the pumping discharge  $Q_w$ , the results are independent of the pumping discharge. In the second comparison the effective parameters calculated for both upscaling methods are compared to optimized values derived from the explicit model. The optimized values are determined by

minimizing, in the least squares sense, the difference between the head in the regional aquifer in the explicit model and in the upscaled model. The results are presented per scenario.

### 4.3.1 Scenario 1

Scenario 1 represents a single-layer phreatic layer with fully penetrating ditches. Table 4.3 shows how well the drawdown in the two upscaled models corresponds with the drawdown observed in the explicit model at three points in the cross-section for each scenario. The first point is at the drain, the next two are at  $\lambda$  and  $2\lambda$ . The parameter  $\lambda$  is also known as the characteristic length and is calculated from the explicit model with

$$\lambda = \sqrt{T_{\text{reg}}c_{\text{opt}}^*} \quad (4.1)$$

where  $T_{\text{reg}} = k_{\text{reg}}H_{\text{reg}}$  is the transmissivity of the regional aquifer and  $c_{\text{opt}}^*$  is the optimized value for  $c^*$ . It is calculated by minimizing, in the least squares sense, the difference in head in the regional aquifer between the explicit model and an upscaled model. At a distance of  $2\lambda$  only 14% of the influence of the extraction remains. As expected, both upscaling methods yield good estimates for the drawdown. The phreatic layer in these scenarios closely resembles the conceptual models from which the upscaling methods were derived.

**Table 4.3:** Drawdown comparison for all scenarios for three points in the cross-section. A value of 1.0 indicates a perfect correspondence between the drawdown calculated by the explicit model and the upscaled model.

Scenario	Drawdown ratio	Comparison points		
		$x = 0$	$\lambda$	$2\lambda$
1	$s_{\text{DL}}/s_{\text{exp}}$	1.004	1.007	1.010
	$s_{\text{ML}}/s_{\text{exp}}$	0.997	0.995	0.991
2	$s_{\text{DL}}/s_{\text{exp}}$	0.993	0.985	0.977
	$s_{\text{ML}}/s_{\text{exp}}$	1.000	0.999	0.998
3	$s_{\text{DL}}/s_{\text{exp}}$	1.010	1.019	1.029
	$s_{\text{ML}}/s_{\text{exp}}$	0.996	0.991	0.987

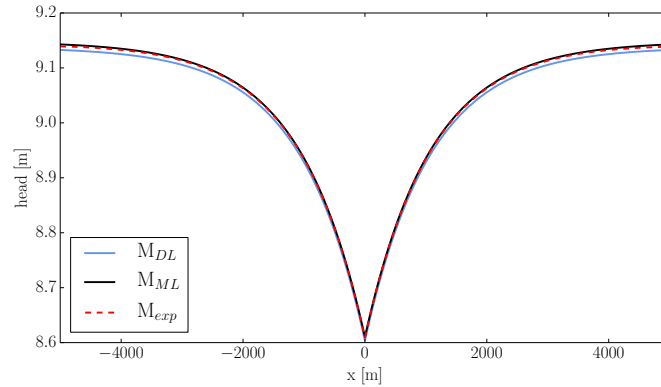
The drawdown indicates whether the shape of the drawdown curve is similar in the upscaled and explicit models but it does not indicate whether the head is accurately estimated. Table 4.4 shows the values for the effective parameters calculated with the upscaling methods and the optimized values for those parameters derived from the explicit model. Differences in the values of the effective parameters are negligible and both upscaling methods perform well.

**Table 4.4:** Values for effective parameters  $p^*$  and  $c^*$  for Scenarios 1-3. The values for the explicit model were determined with an optimization.

Scenario	Parameters [Units]	Upscaled models		
		$M_{exp}$	$M_{DL}$	$M_{ML}$
1	$p^*$ [m]	9.082	9.080	9.083
	$c^*$ [d]	1084	1096	1082
2	$p^*$ [m]	9.146	9.138	9.148
	$c^*$ [d]	1152	1140	1156
3	$p^*$ [m]	9.266	9.374	9.269
	$c^*$ [d]	1351	1397	1358

### 4.3.2 Scenario 2

In Scenario 2 the ditches do not fully penetrate the phreatic layer. Table 4.3 shows differences between de Lange’s upscaling method and the explicit model are in the order of a few percent. The multi-layer upscaling method performs slightly better but differences are negligible. Figure 4.4 shows the head in the regional aquifer for each model. This shows that both upscaling methods accurately account for partial penetration of ditches.



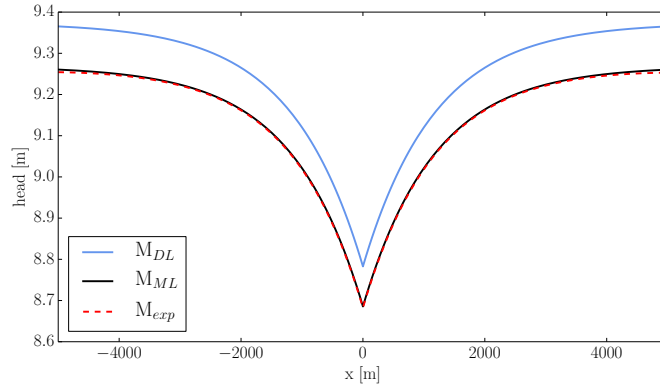
**Figure 4.4:** Groundwater head in the regional aquifer for the explicit model and both upscaled models for Scenario 2 with  $Q_w = 1.0 \text{ m}^2/\text{d}$ .

Table 4.4 shows that the values for the effective parameters are similar, which confirms that both upscaling methods perform well.

### 4.3.3 Scenario 3

In Scenario 3 vertical anisotropy is introduced to the phreatic layer. Table 4.3 shows that the drawdown calculated with the upscaled models is a good estimate of the drawdown in the explicit model. However, the draw-

down does not indicate how well the upscaled models are able to calculate the effective groundwater level ( $p^*$  in the upscaling methods). Figure 4.5 shows the head in the regional aquifer for all three models. De Lange’s upscaling method does not give a good estimate for  $p^*$ .



**Figure 4.5:** Groundwater head in the regional aquifer for the explicit model and both upscaled models for Scenario 3 with  $Q_w = 1.0 \text{ m}^2/\text{d}$ .

Table 4.4 shows that the values for  $c^*$  are similar for all three models, which explains why the drawdown is accurately estimated. The value for  $p^*$  calculated with de Lange’s upscaling method is overestimated. De Lange’s method is not able to accurately account for strong vertical anisotropy.

## 4.4 Discussion

In homogeneous and isotropic phreatic layers both upscaling methods perform well. Differences in the calculated drawdown, as compared with the explicit model, are on the order of 1-2%. The values for the effective parameters ( $p^*$  and  $c^*$ ) are similar. Both methods perform well because the schematization of the phreatic layer in the explicit model is similar to the conceptual models used as a basis for derivations of the two upscaling methods.

When anisotropy is considered de Lange’s method yields a reasonable estimate for  $c^*$  but not for  $p^*$ . The value for  $p^*$  is overestimated significantly because either the formula for the radial resistance is inaccurate for anisotropic conditions, or the method through which the radial resistance is included in de Lange’s formulas is not valid in highly anisotropic phreatic layers.

The three scenarios each represent a different schematization of the phreatic layer, but the parameters defining the geology of the subsurface are the same for all scenarios. These parameters are representative for a clayey subsurface in the Netherlands. The distance between ditches was

set to 100 m, which is larger than many practical settings. Earlier studies show that these conditions are challenging for de Lange's upscaling method. [De Lange \(1997b\)](#) indicates his approach is inaccurate when  $c_0$  is relatively small compared to  $c_1$ , when there is strong anisotropy and when the distances between ditches are large. [Groenendijk et al. \(2002\)](#) confirm anisotropy in combination with large values for  $L$  leads to large differences between the effective parameters calculated by [de Lange \(1999\)](#) and the upscaling method developed by [Kovar and Rolf \(1978\)](#) (a 2D method which is assumed to be more accurate). In Scenario 3, when  $L$  is reduced to 20 m, the effective water level calculated with de Lange differed from the value in the explicit model by ca. 3 cm.

The effect of increasing the transmissivity of the phreatic layer, and decreasing the resistance of the aquitard was also examined. The upscaling methods were compared for parameters representing a peaty subsurface; the hydraulic conductivity in the phreatic layer was set to 5 m/d and the resistance of the aquitard,  $c_1$ , was set to 100 days. The differences between the upscaling methods with these parameter values is negligible for all scenarios.

With highly permeable top systems and relatively small distances between ditches, both methods perform well. However, the multi-layer method yields consistently accurate results, even in top-systems with a lower transmissivity and larger distances between ditches.

The reason the multi-layer method is consistently accurate is because it accounts for anisotropy by including the resistance to vertical flow in the leaky layers below each sub-layer. The inclusion of 10 sub-layers in the phreatic layer, eliminates the need for the radial resistance to be added at a later stage. According to [Groenendijk et al. \(2002\)](#), the empirical justification for the addition of the resistance to vertical flow and the radial resistance, as opposed to a physical justification, is a weakness in de Lange's approach. The multi-layer method eliminates this weakness and therefore the multi-layer method is preferred, especially in low permeable top-systems with significant vertical anisotropy.

## Chapter 5

# Comparison of upscaling methods for phreatic layers with layered heterogeneity

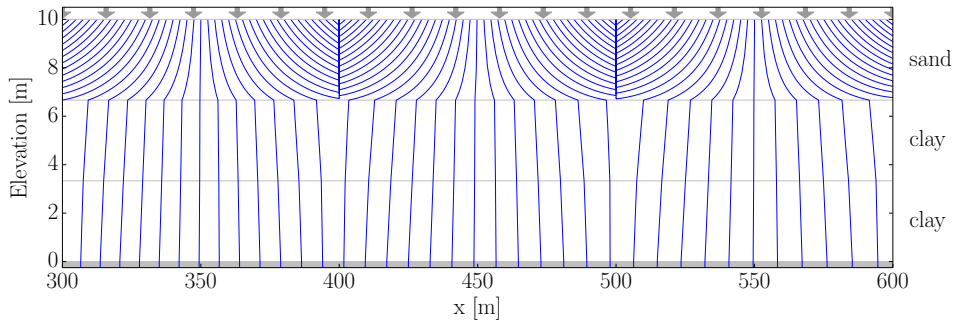
This chapter presents the results of the comparison between upscaled models using the two upscaling methods and the explicit model for heterogeneous phreatic layers. First, the effect of heterogeneity on the flow through the phreatic layer is examined. Section 5.2 describes how the models are set up. The results of the comparisons are presented in Section 5.3. The chapter ends with a discussion on the obtained results.

### 5.1 Flow through heterogeneous phreatic layers

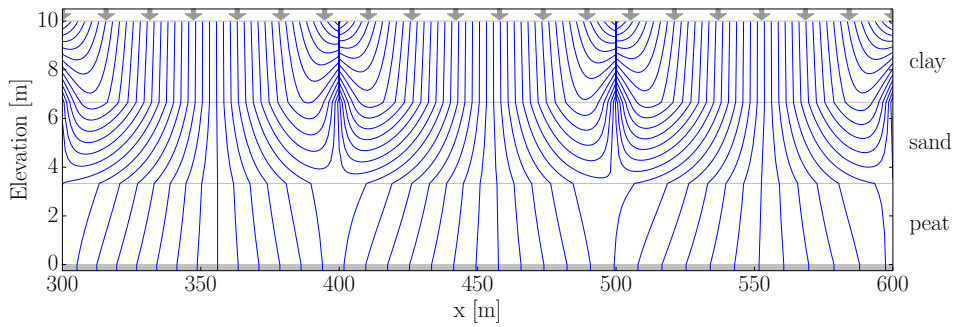
The flow through the phreatic layers with layered heterogeneity is examined to gain insight into the effect of heterogeneity. Several different configurations of the sub-layers of the phreatic layer are examined. Figure 5.1 shows streamlines for a phreatic layer consisting of three sub-layers with sand in the top-most sub-layer. Almost all the flow through the phreatic layer towards the ditches takes place in the sandy layer. In the clay layers the streamlines are nearly vertical. A large portion of the recharge flows towards the ditches, and due to the clay layers, the resistance to flow towards the regional aquifer is significant.

Figure 5.2 shows streamlines for a phreatic layer consisting of clay, sand and peat. The majority of flow towards the ditches takes place in the sandy layer. De Lange's upscaling method depends on  $c_{\text{rad}}$  to account for the partial penetration of ditches and anisotropy. However, the formula derived for radial resistance by Ernst (1962) is valid for homogeneous aquifers. The radial resistance in a layered heterogeneous system is not the same as radial resistance in a homogeneous phreatic layer with an equivalent transmissivity.

Figure 5.3 shows the flow of water through a phreatic layer consisting of



**Figure 5.1:** Streamlines for a heterogeneous phreatic layer with sand, clay and clay sub-layers from top to bottom. The vertical dimension is exaggerated 10×.



**Figure 5.2:** Streamlines for heterogeneous phreatic layer with clay, sand and peat sub-layers from top to bottom. The vertical dimension is exaggerated 10×.

clay in the top two sub-layers and sand at the bottom. Most of the water flows down towards the bottom sub-layer and although some water flows back upwards near the ditches, a lot of it percolates to the regional aquifer. This means that the approximation in the derivation of  $p^*$  that all recharge flows towards the ditches is perhaps no longer justified. The justification of this approximation is discussed in Chapter 6.

Figure 5.4 shows streamlines for a phreatic layer with ten sub-layers. The lithology is shown in Figure 5.5. The fourth sub-layer consists of sand; there is a clear horizontal flow component and a large amount of the infiltrated water flows towards the ditches through this layer.

## 5.2 Description of model set-up

The upscaled models are compared to the explicit model for two schematizations of the phreatic layer with layered heterogeneity. The models are set

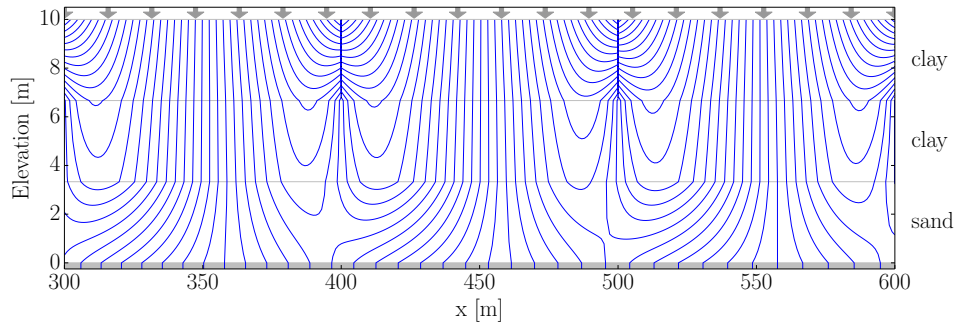


**Figure 5.3:** Streamlines for heterogeneous phreatic layer with clay, clay and sand sub-layers from top to bottom. The vertical dimension is exaggerated  $10\times$ .

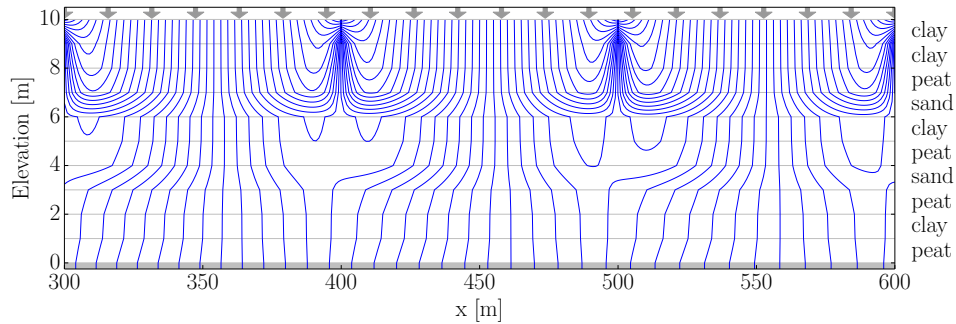


**Figure 5.4:** Streamlines in a heterogeneous phreatic layer with ten sub-layers. The vertical dimension is exaggerated  $10\times$ .

up as described in Section 4.2. The lithology of the subsurface is defined in Figure 5.5 and is the same for both scenarios. The defined soil types are clay, peat and sand with horizontal hydraulic conductivities of 1, 5, and 25 m/d respectively. Table 5.1 summarizes the phreatic layer characteristics for scenarios 4 and 5. The phreatic layer in Scenario 4 is heterogeneous but isotropic, and in Scenario 5, vertical anisotropy is introduced.

## 5.3 Performance of upscaling methods for phreatic layers with layered heterogeneity

### 5.3.1 Scenario 4

Scenario 4 represents a phreatic layer with layered heterogeneity in which the conductivities are isotropic. Table 5.2 presents the drawdown ratio between the upscaled models and the explicit model. For Scenario 4 de Lange's upscaling method underestimates the drawdown by 2% at the drain and 6%

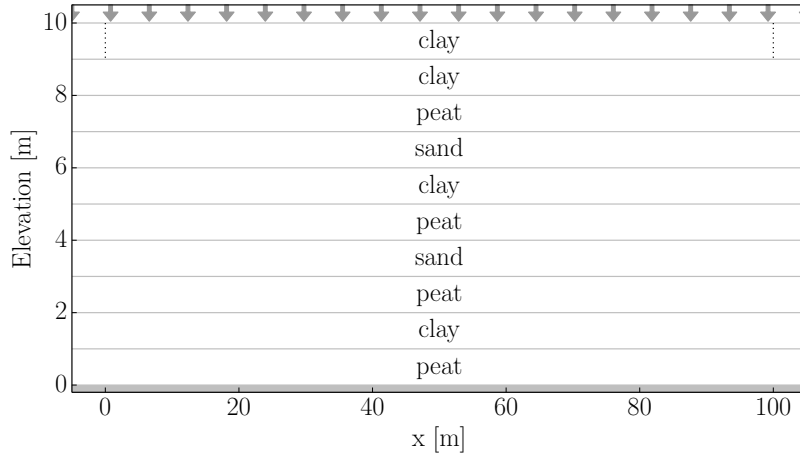


**Figure 5.5:** Heterogeneous lithology of the phreatic layer in Scenarios 4 and 5. The horizontal hydraulic conductivities for clay, peat and sand are 1, 5 and 25 m/d respectively.

**Table 5.1:** Description of the schematization of the phreatic layer for the explicit model. The simplified models are tested against the explicit model for each scenario.

Scenario	Phreatic layer characteristics
4	Heterogeneous phreatic layer consisting of 10 sub-layers. Ditches partially penetrate the phreatic layer, conditions are isotropic
5	Heterogeneous phreatic layer consisting of 10 sub-layers. Ditches partially penetrate the phreatic layer, conditions are anisotropic

at a distance of  $2\lambda$ . The drawdown calculated with the multi-layer upscaling method closely matches the drawdown in the explicit model.

Table 5.3 shows the values of the effective parameters for both upscaling methods and optimized values derived from the explicit model. The value for  $p^*$  calculated with de Lange’s method is about 4 cm lower than the optimized value. The differences for both  $p^*$  and  $c^*$  are small, but the multi-layer upscaling method gives better estimates.

### 5.3.2 Scenario 5

In Scenario 5, vertical anisotropy is reintroduced. Table 5.2 shows that the multi-layer upscaled model yields more accurate estimates for the drawdown in the regional aquifer. De Lange’s upscaled model underestimates the drawdown by 5% at the well, and by 15% at a distance of  $2\lambda$ .

**Table 5.2:** Drawdown comparison for Scenario 4 and 5 for three observation points in the cross-section. A value of 1.0 indicates a perfect correspondence between the drawdown calculated by the explicit model and the upscaled model.

Scenario	Drawdown ratio	Comparison points		
		$x = 0$	$\lambda$	$2\lambda$
4	$s_{DL}/s_{exp}$	0.979	0.958	0.937
	$s_{ML}/s_{exp}$	1.000	1.000	0.999
5	$s_{DL}/s_{exp}$	0.947	0.895	0.845
	$s_{ML}/s_{exp}$	0.998	0.994	0.991

**Table 5.3:** Values for effective parameters  $p^*$  and  $c^*$  for Scenarios 4 and 5. The values for the explicit model were determined with an optimization.

Scenario	Parameters [Units]	Upscaled models		
		$M_{exp}$	$M_{DL}$	$M_{ML}$
4	$p^*$ [m]	9.072	9.031	9.073
	$c^*$ [d]	1074	1032	1077
5	$p^*$ [m]	9.191	9.103	9.193
	$c^*$ [d]	1226	1114	1236

The reason de Lange’s upscaled model underestimates the drawdown in the regional aquifer is because the value of the effective parameter  $c^*$  differs from the optimized value by more than 100 days. Table 5.3 shows the values of the effective parameters for both upscaling methods and the optimized value derived from the explicit model. De Lange’s upscaling method underestimates  $p^*$  by almost 10 cm. De Lange’s method is not able to accurately account for layered heterogeneity and vertical anisotropy.

### 5.3.3 The effect of layered heterogeneity on effective parameter values

The results for Scenarios 4 and 5 indicate that the multi-layer upscaling method performs better when the phreatic layer is heterogeneous, but only a single configuration of the phreatic layer was examined (see Figure 5.5). The effect of different configurations of layered heterogeneity on the values of the effective parameters calculated by both upscaling methods is examined in an explicit model with a phreatic layer consisting of three sub-layers.

The phreatic layer in the explicit model consists of three sub-layers of equal thickness that consist of clay, peat or sand. The ditches fully penetrate the first sub-layer. The resistance of the aquitard ( $c_1$ ) is set to 100 days. The resistance is lowered to analyze whether the approximation of an



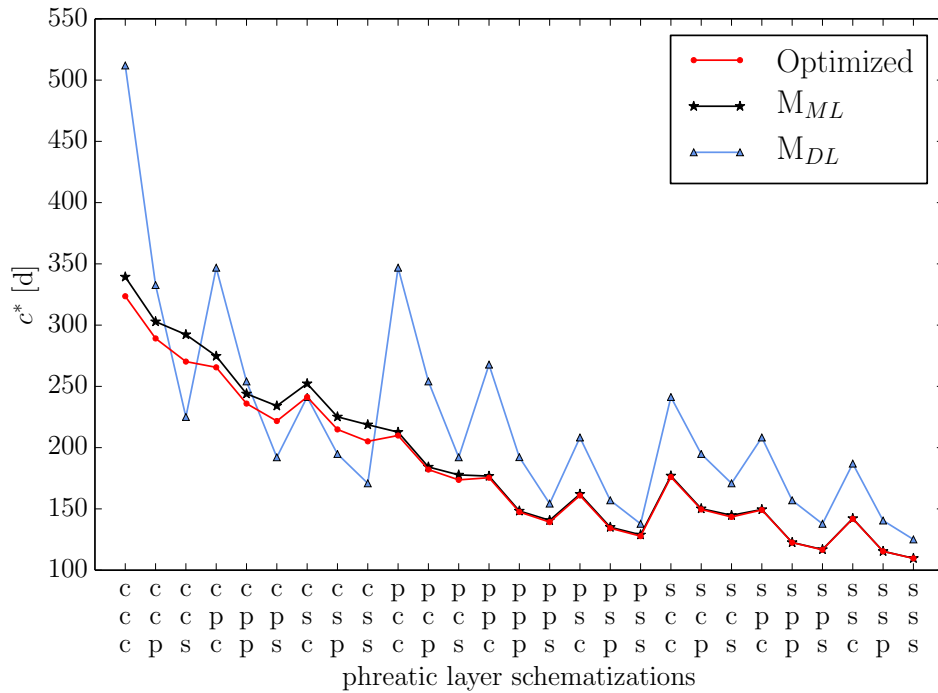


**Figure 5.7:** Comparison of the two upscaling methods for  $c^*$  for all possible lithologies of a phreatic layer consisting of 3 sub-layers. Note that the lines between the points are only included as a visual aid.

sand in the top-most sub-layer, although the values are reasonably accurate for phreatic layers that have a high total transmissivity. The calculated values for  $c^*$  with the multi-layer upscaling method are nearly identical to the optimized values when peat or sand is in the top-most sub-layer. With clay in the first sub-layer, the multi-layer formula overestimates the resistance slightly with differences on the order of 10 days.

### 5.3.4 Sensitivity of drain pumping rate to a prescribed head

The effect of an upscaled model on the value for the pumping rate that is required to satisfy a prescribed head is analyzed. In previous results the pumping rate of the well was specified. Here, the head is prescribed at the drain and the pumping rate is computed such that the prescribed head at the drain is met. The required pumping rate is computed for all models and for all configurations of the 3-layer phreatic layer. The head at the drain is set equal to the elevation of the top of the regional aquifer so that the flow in the regional aquifer remains confined.

Figure 5.8 shows the results of the required pumping rate for the explicit model and both upscaled models for three different values of the resistance

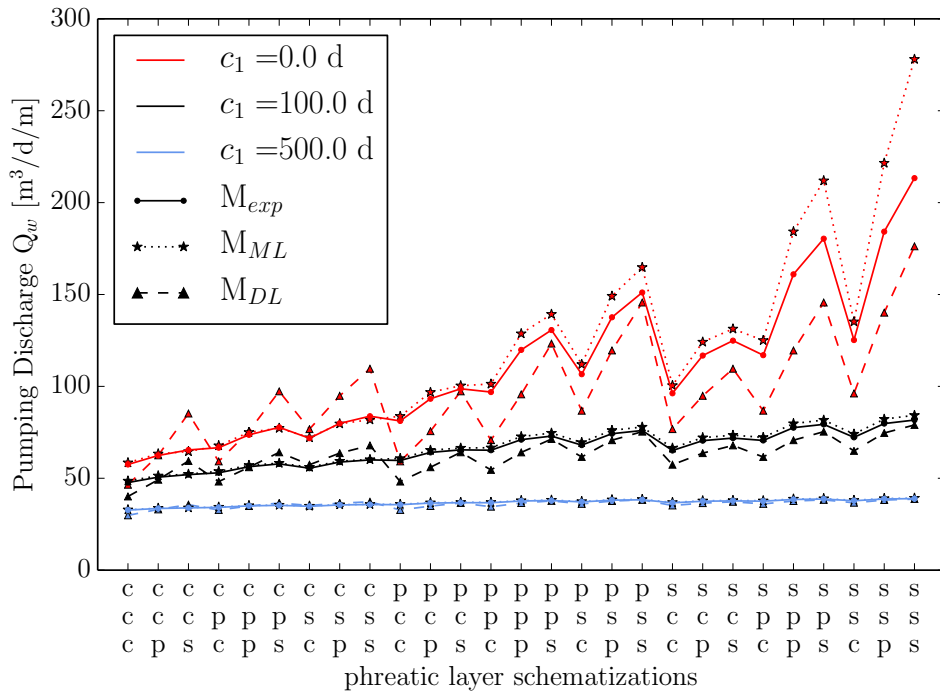


**Figure 5.8:** Pumping rates calculated for a fixed head in the drain for different phreatic layer schematizations with different values for aquitard resistance. Note that the lines between points are only included as a visual aid.

of the aquitard. The multi-layer upscaling method performs well for larger values of  $c_1$ . For smaller  $c_1$ , the multi-layer method performs reasonably well as long as clay or peat are in the top sub-layer. When sand is present in the top sub-layer the maximum discharge is overestimated. De Lange’s method produces more variable results and generally yields worse estimates for smaller values of  $c_1$ . The estimates for the discharge are conservative unless the top sub-layer consists of clay.

### 5.3.5 The effect of semi-random ditch spacing on the effective parameters

Both upscaling methods assume that the ditches are uniformly spaced. In reality the distances between ditches in a drainage network are irregular. An explicit model is created in which the distance between ditches varies between 50, 100, and 200 m to analyze the effect of non-uniform ditch-spacing. The analysis is performed for both a homogeneous and a heterogeneous phreatic layer. A representative value for the distance between the ditches is used in the upscaling formulas to calculate the effective parameters. The

representative distance is different for both upscaling methods.

De Lange (1996) uses the area of the observed region divided by the total length of ditches in that region as the representative distance between ditches. In a cross-section with parallel ditches this simplifies to the width of the observed region divided by the number of ditches, which is the average of the distances between the ditches.

In the multi-layer upscaling method the value of the effective water level is linearly proportional to the mounding between ditches. The mounding between ditches is approximately quadratically proportional to the distance between ditches. An estimate of the representative distance between ditches is then given by

$$L_{\text{rep}} = \sqrt{\frac{\sum L^2}{n}} \quad (5.1)$$

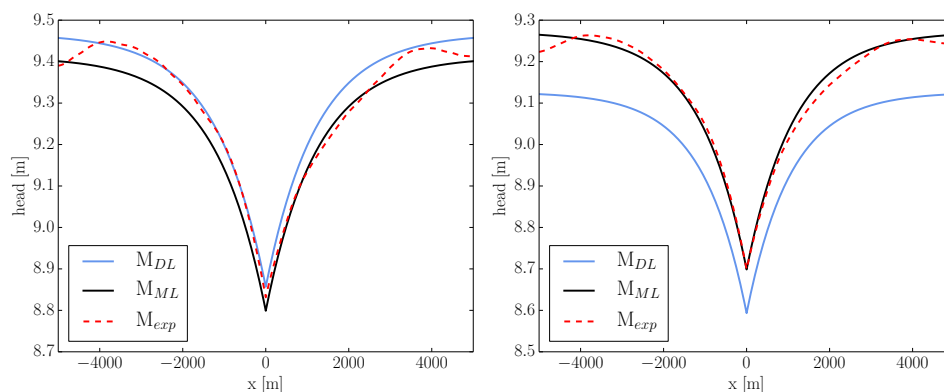


**Figure 5.9:** Head in the regional aquifer for the explicit model, and the two upscaled models for semi-random ditch spacing. The distance between subsequent ditches was randomly selected from 50, 100 or 200 m. The figure on the left was calculated for homogeneous conditions, the one on the right for heterogeneous conditions.

Figure 5.9 shows the head in the regional aquifer with a pumping rate of  $1 \text{ m}^2/\text{d}$  when the distance between subsequent ditches is selected randomly from 50, 100, and 200 m. The left plot shows the results for the homogeneous phreatic layer from Scenario 3. The plot to the right shows the results for the phreatic layer with layered heterogeneity defined in Scenario 5. De Lange’s upscaling method yields a reasonable estimate of the head in homogeneous conditions. In Section 4.3.3 it was shown that de Lange’s formula overestimated the value for  $p^*$  in a homogeneous aquifer with vertical anisotropy. That overestimation seems to compensate for the increase in head due to semi-random ditch spacing, but probably not for the right

reasons. When layered heterogeneity is considered the method no longer yields accurate results.

The multi-layer method performs similar to de Lange in homogeneous conditions and both represent a reasonable average of the head displayed by the explicit model. Obviously, neither method can capture the random patterns that are observed due to the irregular spacing of the ditches. In stretches where the spacing is generally larger, the head in the explicit model is larger, and conversely, when there is a stretch of more closely spaced ditches, the head is lower. In heterogeneous conditions, the multi-layer method yields a much better estimate of the head in the regional aquifer than de Lange's upscaling method.

## 5.4 Discussion

The multi-layer upscaling method performs better than de Lange's formulas when layered heterogeneity and vertical anisotropy are present in the phreatic layer. The figures with streamlines in Section 5.1 show why de Lange's upscaling method is not able to yield accurate results in heterogeneous conditions. The inclusion of a formula for the radial resistance based on a homogeneous aquifer cannot capture the complex flow pattern through the top-system, nor the effective resistance resulting from this flow pattern. De Lange (1997c) created a numerical model of the top-system and cited its ability to take into account layered heterogeneity as one of its advantages. The multi-layer method takes this aspect into account directly in two relatively simple formulas. The approximations that were necessary to derive those formulas appear valid, at least for phreatic layers with the characteristics defined in the previous sections. Chapter 6 contains a more detailed analysis of the limitations of the multi-layer upscaling method.

In the results sections, the values for the effective parameters are compared to optimized values for those parameters derived from the explicit model. The optimized values represent the best possible fit for a top-system consisting of a fixed water level  $p^*$  and a lumped resistance  $c^*$ . However, other optimization criteria, such as the flux in the regional aquifer could lead to different values for the optimized effective parameters. Through visual inspection of the head in the regional aquifer in the explicit model and an upscaled model with the optimized parameters it was determined that this optimization criterion led to good estimates for the optimal values of the effective parameters.

When the required pumping discharge to attain a certain prescribed head in the regional aquifer is calculated with an upscaled model, it is important to know whether a reasonable estimate is obtained. The multi-layer method provides accurate results except for highly permeable top-systems (i.e. the phreatic layer is characterized by a high transmissivity and the aquitard has

a low resistance). In this situation it is better to create an explicit model. De Lange's upscaling method performs reasonably well for larger values of the aquitard resistance but is less accurate than the multi-layer upscaling method because the effective parameters are estimated less accurately.

The multi-layer upscaling method works reasonably well when ditch spacing is semi-random in both homogeneous and heterogeneous conditions. Obviously, the local effects of a region with smaller distances between ditches cannot be accounted for in the upscaled models. Nonetheless, the results are a reasonable average of the head observed in the regional aquifer in the explicit model. De Lange's upscaling method works well in homogeneous conditions with anisotropy but not for the right reasons. The effective water level is generally overestimated by de Lange's method in anisotropic conditions with regular ditch spacing. This overestimation seems to compensate for the increased head caused by the random spacing of ditches.

## Chapter 6

# Limitations of the multi-layer upscaling method

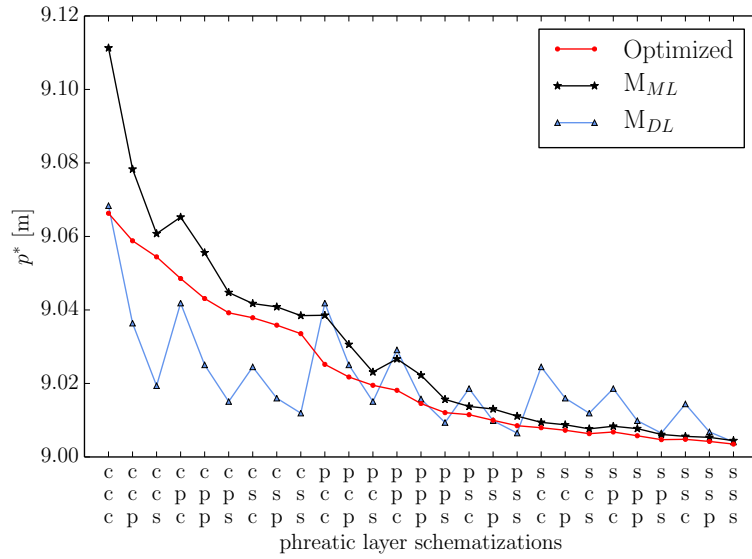
This chapter examines the limitations of the multi-layer upscaling method. These limitations are linked to the approximations that were used in the derivation of this method. Two of the most important approximations are the approximation of an impermeable aquitard in the derivation for  $p^*$  and that recharge does not influence the value of  $c^*$ . Another aspect that warrants more analysis, is how well the upscaling method performs when the bed resistance is not negligible.

### 6.1 Resistance of the aquitard

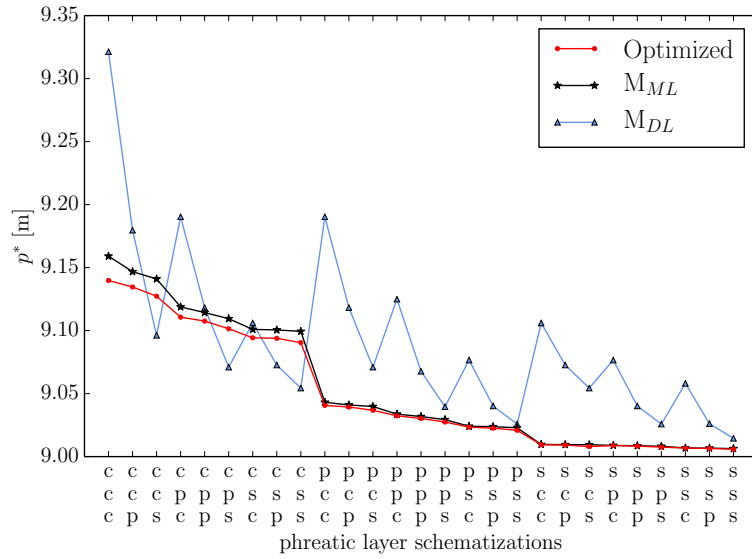
The most important approximation in the derivation for the formula of  $p^*$  is the impermeable boundary at the bottom of the phreatic layer. This approximation is justified as long as the net flux through the bottom of the phreatic layer is small. This flux increases when there is no vertical anisotropy, the resistance of the aquitard is small and the distance between ditches is large.

Figure 6.1b shows the values of  $p^*$  for twenty-seven different phreatic layer configurations calculated by both upscaling methods and the optimal values when the resistance of the aquitard is set to zero. All other phreatic layer characteristics are equal to those defined in Section 5.3.3. Despite the reduced resistance of the aquitard, the formula for  $p^*$  still yields accurate results.

Figure 6.1a shows the values of  $p^*$  for similar conditions but the phreatic layer is isotropic. In this situation, the flux from the phreatic layer to the regional aquifer is larger, especially when the transmissivity of the phreatic layer is low. In these conditions the upscaling formula for  $p^*$  gives less accurate estimates for the effective groundwater level (the largest error is  $\sim 5$  cm).



(a)



(b)

**Figure 6.1:** Comparison of the two upscaling formulas for  $p^*$  in isotropic conditions (a) and anisotropic conditions (b) for all possible lithologies of a phreatic layers consisting of 3 sub-layers with  $c_1 = 0$  d. Note that the lines connecting the points are only included as a visual aid.

In reality drain spacing is lower than 100 m in low permeable phreatic layers (without an aquitard), which means the flux from the phreatic layer to the regional aquifer is smaller. In addition, conditions are rarely isotropic,

which means that in most practical cases the multi-layer upscaling method will yield reasonable results.

## 6.2 Recharge

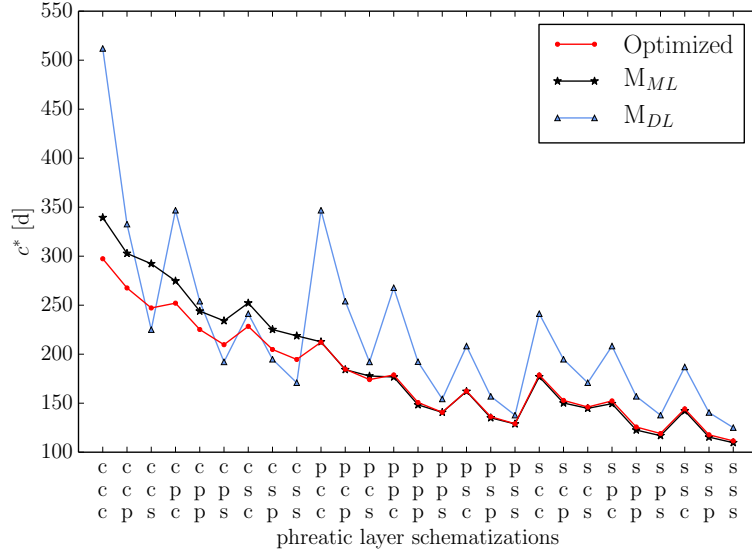


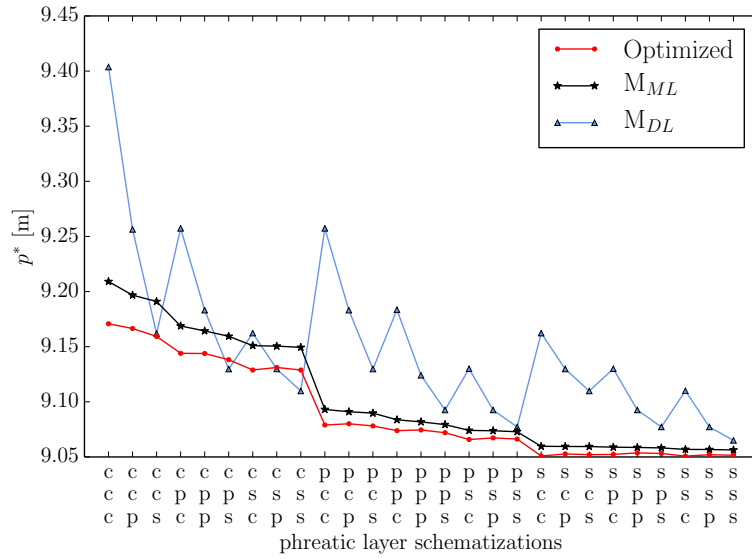
**Figure 6.2:** Comparison of the two upscaling formulas for  $c^*$  for all possible lithologies of a phreatic layers consisting of 3 sub-layers with  $R = 0.01$  m/d. Note that the lines connecting points are only included as a visual aid.

The conceptual model from which the formula for  $c^*$  was derived does not include recharge. Figure 6.2 shows the effect of increasing recharge by a factor ten on the calculation of  $c^*$ . A tenfold increase in recharge represents a yearly rainfall amount of more than 3 m which is well above the actual rainfall in The Netherlands. In conclusion, recharge does not impose a limitation on the accurate estimation of  $c^*$ .

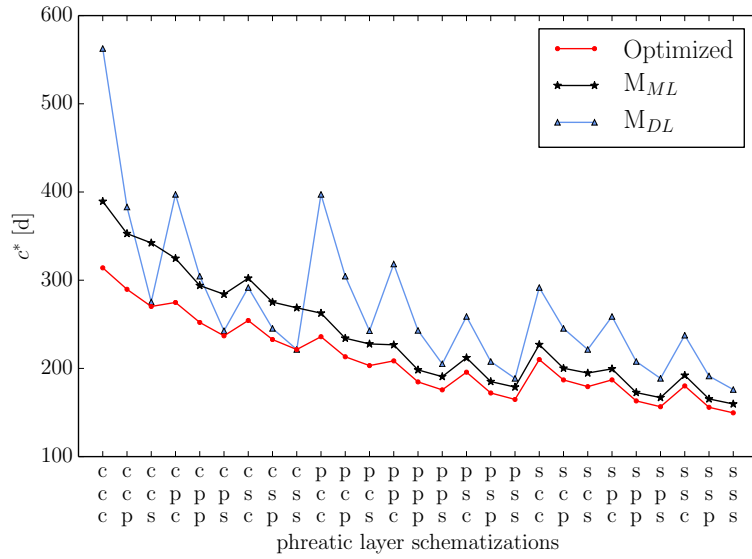
## 6.3 Bed resistance of ditches

The bed resistance of a ditch is taken into account in the multi-layer upscaling method through addition of the head required to flow through this added resistance layer. This approach assumes that the distribution of flow in the phreatic layer does not change. When ratio between the bed resistance and the resistance of the aquitard increases more water will flow through the aquitard, and this renders the multi-layer upscaling formulas less accurate.

Figure 6.3a shows how well the multi-layer upscaling method is able to calculate  $p^*$  when the bed resistance of the ditches is set to 1 day. The



(a)



(b)

**Figure 6.3:** Comparison of the two upscaling formulas for  $p^*$  for all possible lithologies of a phreatic layers consisting of 3 sub-layers with  $c_0 = 1$  d. Note that the lines connecting points are only included as a visual aid.

resistance of the aquitard is 100 days. Although the upscaling formula is still a reasonable estimate of the value for  $p^*$  the difference with the optimized values is much larger than in the situation with zero bed resistance.

Figure 6.3b shows how well the upscaling formula for  $c^*$  performs when

bed resistance is set to 1 day. The largest differences between the multi-layer upscaling method and the optimized values are nearly 100 days. In practice, the value of the bed resistance of a ditch may be as high as a few days. The multi-layer upscaling formulas become less accurate when the bed resistance is more than 1 day while the resistance of the aquitard is 100 days. When the resistance of the aquitard is larger, the upscaling formulas also work for larger values of the bed resistance.

## Chapter 7

# Discussion and conclusions

The purpose of this research was to develop an upscaling method capable of taking into account layered heterogeneity and vertical anisotropy of the top-system and compare that method to the method developed by de Lange. An upscaled model was calculated for each method and compared to an analytic element model containing all features explicitly. In Chapter 2 a new multi-layer upscaling method was derived that takes these aspects into account directly. The derived formulas for  $p^*$  and  $c^*$  depend only on the characteristics of the subsurface. For phreatic layers with more than 2 sub-layers the eigenvalues and eigenvectors need to be determined using numerical methods.

In Chapters 4 and 5 the multi-layer method was compared with an existing method derived by de Lange (1996). The comparison was made using the cross-sectional analytic element model environment described in Chapter 3. A reference model was created in which the phreatic layer and all the ditches it contained were modeled explicitly. The performance of the two upscaling methods was examined by comparing two upscaled models (one for each upscaling method) to the explicit model. The head was compared for a drain in the regional aquifer for different schematizations of the phreatic layer. The effective parameters calculated with both upscaling methods were compared to optimized parameters derived from the explicit model.

The multi-layer upscaling method performs as well as de Lange's method for isotropic and homogeneous phreatic layers. When anisotropy is introduced to the top-system, the multi-layer upscaling method yields more accurate estimates for the effective parameters. For de Lange's method, anisotropy, especially in combination with low transmissivities in the phreatic layer and large distances between ditches, leads to an overestimation of the effective water level. For anisotropic top-systems characterized by a higher transmissivity both models perform equally well.

When layered heterogeneity and vertical anisotropy are present in the top-system, the multi-layer upscaling method is preferred. The calculated

effective parameters are much closer to the optimized values. In those same conditions, performance of de Lange's method varies, with differences increasing as the overall transmissivity of the phreatic layer decreases.

Although the multi-layer upscaling method yields improved estimates for the effective parameters, it does have its limitations. For example, the multi-layer upscaling method cannot be used in areas with wide ditches. The conceptual model forming the basis of the derivation for the multi-layer formulas assumes the width of the ditches is negligible compared to the distance between the ditches (similar to the approach based on Ernst described in [Groenendijk et al. \(2002\)](#)). The values for the effective parameters under a water body are different to those found for the region between them and as these water bodies get wider, the influence of this region increases. De Lange's conceptual model does take these regions into account but its performance was not examined.

Another limitation is that the multi-layer method is not applicable when values for the bed resistance are large relative to the resistance of the aquitard. In this situation the flow pattern through the phreatic layer is significantly altered by the bed resistance, which means the approximations in the derivation of the effective parameters are no longer justified. However, for small values of the bed resistance the multi-layers formulas that take into account the bed resistance are applicable. De Lange's approach allows larger ranges of the bed resistance to be taken into account directly, but its performance was not examined.

Perhaps the most important limitation of the multi-layer method is the amount of data required about the subsurface. The phreatic layer is highly complex and detailed measurements of the characteristics of the sub-layers are difficult and expensive. If data is lacking, the effective parameters will have to be calibrated. The upscaling formulas might then be used to determine a calibration range. However, if the data describes a homogeneous phreatic layer, the multi-layer method still yields accurate results, comparable to the results obtained with de Lange's upscaling method with the advantage of not having to find the correct expression for the radial resistance. Another option, of course, as [Maas \(2008\)](#) also points out, is to use the analytic element method to create an explicit model of the subsurface, which requires more work to implement, but does yield the most accurate results.

Future research is needed to expand the multi-layer upscaling method to situations with relatively wide ditches, to areas with very few ditches, to 2D systems where ditches are not infinitely long and evenly spaced, and to transient systems.

# References

- Ad hoc Werkgroep Consensus Hydrologie (2002). De parameterisatie van de interactie tussen grondwater en oppervlaktewater voor landelijke en regionale grondwatermodellering. *Stromingen*, 8(2):5–9.
- Bakker, M. and Kelson, V. A. (2009). Writing analytic element programs in Python. *Ground Water*, 47(6):828–834.
- Bakker, M. and Strack, O. D. L. (2003). Analytic elements for multiaquifer flow. *Journal of Hydrology*, 271(1-4):119–129.
- de Lange, W. J. (1996). *Groundwater modeling of large domains with analytic elements*. PhD thesis, Delft University of Technology.
- de Lange, W. J. (1997a). Nieuwe inzichten in het gebruik van voedingsweerstand of drainage- leerstand in de randvoorwaarde van een grondwatermodel. Deel 1. *Stromingen*, 3(2):18–28.
- de Lange, W. J. (1997b). Nieuwe inzichten in het gebruik van voedingsweerstand of drainageweerstand in de randvoorwaarde van een grondwatermodel. Deel 2. *Stromingen*, 3(3):31–47.
- de Lange, W. J. (1997c). Nieuwe inzichten in het gebruik van voedingsweerstand of drainageweerstand in de randvoorwaarde van een grondwatermodel. Deel 3. *Stromingen*, 3(4):43–56.
- de Lange, W. J. (1999). A Cauchy boundary condition for the lumped interaction between an arbitrary number of surface waters and a regional aquifer. *Journal of Hydrology*, 226:250–261.
- Dufour, F. C. (2000). *Groundwater in the Netherlands, Facts and figures*. TNO, Delft/Utrecht.
- Ernst, L. F. (1962). Groundwater flow in the saturated zone and its calculation when horizontal parallel open conduits are present. *Verslagen van landbouwkundige onderzoekingen*, (67.15).

- Groenendijk, P., de Lange, W. J., and Kovar, K. (2002). Modelconcepten voor de interactie tussen verzadigd grondwater en oppervlaktewater. *Stromingen*, 8(2):11–28.
- Hemker, C. J. (1984). Steady groundwater flow in leaky multiple-aquifer systems. *Journal of Hydrology*, 72:355–374.
- Hunt, B. (1986). Solutions for steady groundwater flow in multi-layer aquifer systems. *Transport in Porous Media*, 1:419–429.
- Kovar, K. and Rolf, H. (1978). Analytical solution of the recharge of an aquifer from the overlying semi-permeable top-layer with partially penetrating ditches to be used in a numerical model. Technical report, National Institute for Water Supply, Leidschendam.
- Maas, K. (2008). Drainageweerstand en voedingsweerstand van een freatische aquifer. *Stromingen*, 14(2):3–16.
- Strack, O. D. L. (2003). Theory and applications of the Analytic Element Method. *Reviews of Geophysics*, 41(2):1005.
- Sutanudjaja, E. H. (2008). Uncertainty of groundwater models due to different confining layer schematizations. Master’s thesis, Delft University of Technology.
- van Drecht, G. (1983). Calculation of steady groundwater flow to ditches. Technical report, National Institute for Water Supply.
- van Drecht, G. (1997). Modellen voor diffuse ontwatering in de toplaag. *Stromingen*, 3(2):5–16.
- Vergoesen, A. J. J., de Lange, W. J., Veldhuizen, A. A., van Bakel, P. J. T., and Pastoors, M. J. H. (2008). Bepaling van freatische lekweerstanden in het NHI fase 1+. *Stromingen*, 14(4):37–46.

## Appendix A

# De Lange's derivation of the Cauchy boundary condition

This appendix contains a detailed derivation of the method to lump the effects of many small ditches into a simple boundary condition as presented in [de Lange \(1999\)](#). First, the differential equations governing groundwater flow are set up for the conceptual model proposed by [de Lange](#). Next, the boundary conditions are presented and used to solve the differential equation. Finally, the solutions from the two regions (the stretch between ditches and the stretch under a ditch) are combined to calculate the total flux between groundwater and surface water.

Note that the symbols used in this derivation are based on [de Lange \(1999\)](#) and differ slightly from the symbols used in the report. See [Figure 2.3](#) for an explanation of the symbols.

### A.1 The differential equations and boundary conditions

The head in the conceptual model is governed by two differential equations. One for the region  $x \geq 0$  and one for the region  $x \leq 0$ . By setting up a mass balance (water balance) for a small rectangular element in that region with width  $\Delta x$ , the differential equation can be determined. The density of the water is assumed to be constant so that the mass balance is the same as the water balance. The in and out-flow from the element are assumed to be equal, therefore no storage takes place in the element; the system is in steady-state. First, we will take a look at the area  $x \leq 0$ . For region on the left from  $x = -B/2$  to  $x = 0$  the water balance is:

$$\text{In} = \text{Out}$$

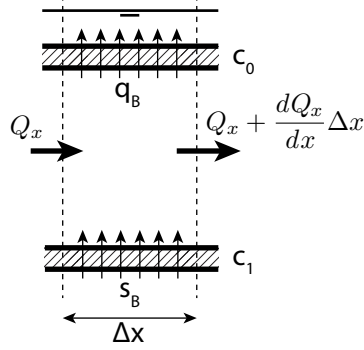


**Figure A.1:** All fluxes flowing into and out of an element with width  $\Delta x$  in the stretch  $-B/2 \leq x \leq 0$

$$\begin{aligned}
 Q_x + s_B \Delta x &= Q_x + \frac{dQ_x}{dx} \Delta x + q_B \Delta x \\
 \frac{dQ_x}{dx} &= s_B - q_B
 \end{aligned} \tag{A.1}$$

Using Darcy's Law and substituting into (Eq. (A.1)) yields:

$$\text{Darcy's Law: } q_x = -kH \frac{dh}{dx} \tag{A.2}$$

$$\frac{d}{dx} \left( -kH \frac{dh}{dx} \right) = s_B - q_B \tag{A.3}$$

We assume the transmissivity  $kH$  is constant in the x-direction so it can be taken out of the differential term.

$$-kH \frac{d^2 h}{dx^2} = s_B - q_B$$

Fluxes  $s_B$  and  $q_B$  can be expressed as functions of the head above and below the leaky layers and the resistance of that leaky layer as seen in Figure A.2.

$$\begin{aligned}
 s_B &= \frac{\phi - h}{c_1} \\
 q_B &= \frac{h - p}{c_0}
 \end{aligned}$$

Substituting in the above relations we get the following differential equation:

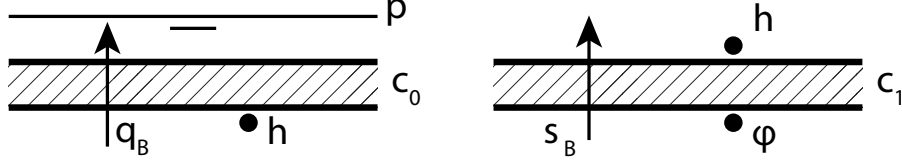


**Figure A.2:** Schematizations of the fluxes through the leaky layers.

$$-kH \frac{d^2 h}{dx^2} = \frac{\phi - h}{c_1} - \frac{h - p}{c_0} \quad (\text{A.4})$$

This differential equation can be rewritten into a more general form:

$$\begin{aligned} kH \frac{d^2 h}{dx^2} &= \frac{h - p}{c_0} - \frac{\phi - h}{c_1} \\ kH \frac{d^2 h}{dx^2} &= \frac{hc_1 - pc_1 + \phi c_0 - hc_0}{c_0 c_1} \\ \frac{d^2 h}{dx^2} &= \frac{h(c_1 + c_0) - c_1 p + c_0 \phi}{kH c_0 c_1} \\ \frac{d^2 h}{dx^2} &= \frac{h - \frac{c_1 p + c_0 \phi}{c_1 + c_0}}{\frac{kH c_0 c_1}{c_1 + c_0}} \\ \frac{d^2 h}{dx^2} &= \frac{h - t_B}{\lambda_B^2} \end{aligned} \quad (\text{A.5})$$

with:

$$t_B = \frac{c_1 p + c_0 \phi}{c_1 + c_0} \quad (\text{A.6})$$

$$\lambda_B = \sqrt{\frac{kH c_0 c_1}{c_1 + c_0}} \quad (\text{A.7})$$

This is the final form of the differential equation for  $-B/2 \leq x \leq 0$  which will be solved in section [A.2](#).

Next we take a look at the region where  $x \geq 0$ , more specifically where  $0 \leq x \leq L/2$ . The water balance for the region with width  $\Delta x$  from Figure [A.3](#) is written below. For reasons that are unclear, de Lange opted to make the recharge  $R$  negative when water is flowing into the system.

$$\begin{aligned} -R\Delta x + Q_x + s_L \Delta x &= Q_x + \frac{dQ_x}{dx} \Delta x \\ \frac{dQ_x}{dx} &= s_L - R \end{aligned}$$

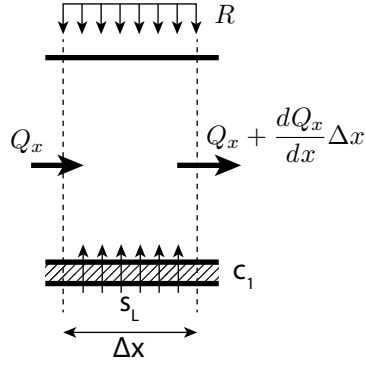


**Figure A.3:** All fluxes for an element with width  $\Delta x$  in the stretch  $0 \leq x \leq L/2$ .

Once again using Darcy's Law (Eq. A.2) and assuming the transmissivity  $kH$  to be constant in the  $x$  direction results in the following differential equation.

$$-kH \frac{d^2 h}{dx^2} = s_L - R$$

The flux  $s_L$  is also equal to the difference in head over the leaky layer divided by the resistance of that leaky layer.

$$s_L = \frac{\phi - h}{c_1}$$

Which yields the following equation. This equation can be rewritten into the same form as the differential equation for the region  $x \leq 0$ .

$$\begin{aligned} kH \frac{d^2 h}{dx^2} &= R - \frac{\phi - h}{c_1} \\ kH \frac{d^2 h}{dx^2} &= \frac{c_1 R - \phi + h}{c_1} \\ \frac{d^2 h}{dx^2} &= \frac{h - (\phi - Rc_1)}{kHc_1} \\ \frac{d^2 h}{dx^2} &= \frac{h - t_L}{\lambda_L^2} \end{aligned} \tag{A.8}$$

where:

$$t_L = \phi - c_1 R \tag{A.9}$$

$$\lambda_L = \sqrt{kHc_1} \tag{A.10}$$

The boundary conditions for this problem are

1. Water divides at  $x = -B/2$  and  $x = L/2$  as a result of the symmetry of the original model.
2. Continuity of flow at  $x = 0$ . The amount of water flowing through the "boundary" at  $x = 0$  should be equal in both solutions. Similarly, the calculated head should be equal.

Mathematically these four boundary conditions can be expressed as follows

$$\frac{dh}{dx} = 0 \quad \text{at } x = -\frac{B}{2} \quad (\text{A.11})$$

$$\frac{dh}{dx} = 0 \quad \text{at } x = \frac{L}{2} \quad (\text{A.12})$$

$$\left. \frac{dh}{dx} \right|_{\text{left}} = \left. \frac{dh}{dx} \right|_{\text{right}} \quad \text{at } x = 0 \quad (\text{A.13})$$

$$h_{\text{left}} = h_{\text{right}} \quad \text{at } x = 0 \quad (\text{A.14})$$

## A.2 Solution of the differential equations and calculating constants

The general form of the differential equation that describes the head in the top aquifer is shown below.

$$\frac{d^2h}{dx^2} = \frac{h - t_i}{\lambda_i^2} \quad \text{where } i = B, L \quad (\text{A.15})$$

The homogeneous equation is

$$h'' - \frac{h}{\lambda_i^2} = 0 \quad (\text{A.16})$$

The second derivative of a function minus the function itself divided by a factor should equal 0. Therefore we assume a solution of the form  $f(x) = \exp(rx)$ . The second and first derivatives of this function are

$$\begin{aligned} f'(x) &= r \exp(rx) \\ f''(x) &= r^2 \exp(rx) \end{aligned}$$

Plugging these solutions into (Eq. A.16) we get

$$r^2 \exp(rx) - \frac{\exp(rx)}{\lambda_i^2} = 0$$

$$\exp(rx) \left( r^2 - \frac{1}{\lambda_i^2} \right) = 0$$

Dividing by  $\exp(rx) (\neq 0)$  results in

$$r^2 - \frac{1}{\lambda_i^2} = 0$$

$$r = \pm \frac{1}{\lambda_i}$$

Therefore the solution to the homogeneous differential equation is a linear combination of the two possible solutions each multiplied by a constant.

$$h(x) = C_{1,i} \exp\left(\frac{-x}{\lambda_i}\right) + C_{2,i} \exp\left(\frac{x}{\lambda_i}\right) \quad (\text{A.17})$$

To get the final solution to the differential equation we have to find the non-homogeneous solution, or particular solution for the following equation

$$h'' - \frac{h}{\lambda_i^2} = \frac{-t_i}{\lambda_i^2} \quad (\text{A.18})$$

Since the term on the right-hand-side is a constant we try a polynomial as a solution

$$g(x) = Ax^2 + Bx + C$$

$$g'(x) = 2Ax + B$$

$$g''(x) = 2A$$

Plugging in this solution into (Eq. (A.18)) yields

$$2A\lambda_i^2 - Ax^2 - Bx - C = -t_i$$

Since there are no terms with  $x^2$  or  $x$  on the RHS we can state that A and B must be equal to zero leaving us with

$$C = t_i$$

The final solution becomes

$$\boxed{h(x) = C_{1,i} \exp\left(\frac{-x}{\lambda_i}\right) + C_{2,i} \exp\left(\frac{x}{\lambda_i}\right) + t_i} \quad (\text{A.19})$$

Using the boundary conditions given in equations (A.11)-(A.14) the coefficients  $C_{1,B}$ ,  $C_{2,B}$ ,  $C_{1,L}$  and  $C_{2,L}$  can be calculated. Differentiating the final solution with respect to  $x$  yields the following expression

$$\frac{dh}{dx} = -\frac{C_{1,i}}{\lambda_i} \exp\left(\frac{-x}{\lambda_i}\right) + \frac{C_{2,i}}{\lambda_i} \exp\left(\frac{x}{\lambda_i}\right) \quad (\text{A.20})$$

Using the first boundary condition (A.11) we get

$$-\frac{C_{1,B}}{\lambda_B} \exp\left(\frac{B}{2\lambda_B}\right) + \frac{C_{2,B}}{\lambda_B} \exp\left(\frac{-B}{2\lambda_B}\right) = 0$$

$$\boxed{C_{1,B} = C_{2,B} \exp\left(\frac{-B}{\lambda_B}\right)} \quad (\text{A.21})$$

Similarly, using the second boundary condition (A.12) we get the following solution for the constant  $C_{1,L}$

$$-\frac{C_{1,L}}{\lambda_L} \exp\left(\frac{-L}{2\lambda_L}\right) + \frac{C_{2,L}}{\lambda_L} \exp\left(\frac{L}{2\lambda_L}\right) = 0$$

$$\boxed{C_{1,L} = C_{2,L} \exp\left(\frac{L}{\lambda_L}\right)} \quad (\text{A.22})$$

Using the fourth boundary condition (Eq. A.14) and substituting in equations (A.21) and (A.22) yields

$$\begin{aligned} C_{2,B} \exp\left(\frac{-B}{\lambda_B}\right) + C_{2,B} + t_B &= C_{2,L} \exp\left(\frac{L}{\lambda_L}\right) + C_{2,L} + t_L \\ C_{2,B} &= \frac{C_{2,L} \left(\exp\left(\frac{L}{\lambda_L}\right) + 1\right) + t_L - t_B}{\left(\exp\left(\frac{-B}{\lambda_B}\right) + 1\right)} \end{aligned} \quad (\text{A.23})$$

We introduce the following helper variables

$$\alpha_B = \exp\left(\frac{-B}{\lambda_B}\right)$$

$$\alpha_L = \exp\left(\frac{L}{\lambda_L}\right)$$

The expression for  $C_{2,B}$  becomes

$$C_{2,B} = \frac{C_{2,L}(\alpha_L + 1) + t_L - t_B}{(\alpha_B + 1)} \quad (\text{A.24})$$

The third boundary condition states that the flow at  $x = 0$  on the left and on the right must be equal (equation (A.13)). Differentiating the final solutions with respect to  $x$  and plugging in the equations for  $C_{1,B}$  and  $C_{1,L}$  yields the following equation

$$\begin{aligned} \frac{-C_{1,B}}{\lambda_B} + \frac{C_{2,B}}{\lambda_B} &= \frac{-C_{1,L}}{\lambda_L} + \frac{C_{2,L}}{\lambda_B} \\ \frac{-C_{2,B}}{\lambda_B} \left(1 - \exp\left(\frac{-B}{\lambda_B}\right)\right) &= \frac{-C_{2,L}}{\lambda_L} \left(1 - \exp\left(\frac{L}{\lambda_L}\right)\right) \\ \frac{-C_{2,B}}{\lambda_B} (1 - \alpha_B) &= \frac{-C_{2,L}}{\lambda_L} (1 - \alpha_L) \end{aligned} \quad (\text{A.25})$$

Plugging the equation for  $C_{2,B}$  (equation (A.24)) into equation (A.25) allows us to solve for  $C_{2,L}$ .

$$\begin{aligned} \frac{C_{2,L}(\alpha_L + 1) + t_L - t_B}{\lambda_B(\alpha_B + 1)} \cdot (1 - \alpha_B) &= \frac{C_{2,L}(1 - \alpha_L)}{\lambda_L} \\ [C_{2,L}\lambda_L(\alpha_L + 1) + \lambda_L(t_L - t_B)] \cdot (1 - \alpha_B) &= C_{2,L}\lambda_B(1 - \alpha_L)(\alpha_B + 1) \\ C_{2,L}[\lambda_L(\alpha_L + 1)(1 - \alpha_B) - \lambda_B(1 - \alpha_L)(\alpha_B + 1)] &= -\lambda_L(t_L - t_B)(1 - \alpha_B) \\ C_{2,L} &= \frac{-\lambda_L(t_L - t_B)(1 - \alpha_B)}{\lambda_L(\alpha_L + 1)(1 - \alpha_B) - \lambda_B(1 - \alpha_L)(\alpha_B + 1)} \end{aligned}$$

Rearrangement of some variables finally yields the following expression for  $C_{2,L}$ .

$$C_{2,L} = \frac{\lambda_L(t_B - t_L)(\alpha_B - 1)}{\lambda_L(\alpha_L + 1)(\alpha_B - 1) - \lambda_B(\alpha_L - 1)(\alpha_B + 1)} \quad (\text{A.26})$$

Substitution of the above equation into (A.24) to solve for  $C_{2,B}$  eventually yields

$$C_{2,B} = \frac{\lambda_B(t_B - t_L)(\alpha_L - 1)}{\lambda_L(\alpha_L + 1)(\alpha_B - 1) - \lambda_B(\alpha_L - 1)(\alpha_B + 1)} \quad (\text{A.27})$$

### A.3 Flux from regional aquifer to the top system per region

The previous section presents the solutions to the differential equations and solved for all the constants. With this information we can find an expression for the total flux to or from surface water for our model. To find this flux, first the fluxes for the two different regions must be determined individually before they are combined into one expression. First, we will take a look at the stretch  $0 \leq x \leq L/2$ . To calculate the flux we make use of the following formula:

$$s = \frac{\phi_i - h_{i,av}}{c_1}$$

This equation will be rewritten into an expression containing lumped parameters:  $p_i^*$  and  $c_i^*$ .

$$s = \frac{\phi_i - p_i^*}{c_i^*}, \quad \text{where } i = B, L$$

#### A.3.1 Lumped parameters for area between $0 \leq x \leq L/2$

The average head in the top aquifer is found by integrating the solution for  $h$  (equation A.19) over the stretch from 0 to  $L/2$  and dividing by the total length of that stretch.

$$\begin{aligned} h_{av,L} &= \frac{2}{L} \int_0^{L/2} h_L dx \\ &= \frac{2}{L} \int_0^{L/2} C_{1,L} \exp\left(\frac{-x}{\lambda_L}\right) + C_{2,L} \exp\left(\frac{x}{\lambda_L}\right) + t_L dx \\ &= \frac{2}{L} \left[ -\lambda_L \alpha_L C_{2,L} \exp\left(\frac{-x}{\lambda_L}\right) + \lambda_L C_{2,L} \exp\left(\frac{x}{\lambda_L}\right) + t_L x \right]_0^{L/2} \\ &= \frac{2}{L} \left[ -\lambda_L \alpha_L C_{2,L} \exp\left(\frac{-L}{2\lambda_L}\right) + \lambda_L C_{2,L} \exp\left(\frac{L}{2\lambda_L}\right) + \frac{t_L L}{2} \right. \\ &\quad \left. - (-\lambda_L \alpha_L C_{2,L} + \lambda_L C_{2,L}) \right] \end{aligned}$$

Because  $\exp\left(\frac{L}{2\lambda_L}\right) - \alpha_L \exp\left(\frac{-L}{2\lambda_L}\right) = 0$  we get:

$$\boxed{h_{av,L} = \frac{2\lambda_L C_{2,L} (\alpha_L - 1)}{L} + t_L} \quad (\text{A.28})$$

The Cauchy boundary condition describes the flux to or from the regional aquifer. Substitution of the expression above for  $h_{av,L}$  and rewriting yields a simple expression for the flux in the region between ditches. These new

parameters,  $c_L^*$  and  $p_L^*$  are independent of the head in the regional aquifer  $\phi$ . All the data from the original model is still accounted for in the simplified expression.

$$s_L = \frac{\phi - h_{av,L}}{c_1} \quad \rightarrow \quad s_L = \frac{\phi - p_L^*}{c_L^*}$$

The following steps show how we get from the expression above on the left to the expression above on the right. The goal is to find expressions for  $c_L^*$  and  $p_L^*$ .

$$s_L = \frac{\phi}{c_1} - \frac{2\lambda_L C_{2,L} (\alpha_L - 1)}{L c_1} - \frac{t_L}{c_1}$$

Substituting in equation (A.26) for  $C_{2,L}$  and using the following helper variable

$$M = \lambda_L (\alpha_L + 1) (\alpha_B - 1) - \lambda_B (\alpha_L - 1) (\alpha_B + 1)$$

$$\begin{aligned} s_L &= \frac{\phi}{c_1} - \frac{2\lambda_L^2 (t_B - t_L) (\alpha_L - 1) (\alpha_B - 1)}{c_1 M L} - \frac{t_L}{c_1} \\ &= \frac{\phi M L - 2\lambda_L^2 (t_B - t_L) (\alpha_L - 1) (\alpha_B - 1) - t_L M L}{c_1 M L} \\ &= \frac{\phi M L - 2\lambda_L^2 \left( \frac{c_1 p + c_0 \phi}{c_1 + c_0} - \phi + R c_1 \right) (\alpha_L - 1) (\alpha_B - 1) - (\phi - R c_1) M L}{c_1 M L} \cdot \frac{(c_1 + c_0)}{(c_1 + c_0)} \\ &= \frac{-2\lambda_L^2 (p - \phi + R(c_1 + c_0)) (\alpha_L - 1) (\alpha_B - 1) + R(c_1 + c_0)}{(c_1 + c_0) M L} \\ &= \frac{-p + \phi - R(c_1 + c_0) + \frac{R(c_1 + c_0) M L}{2\lambda_L^2 (\alpha_L - 1) (\alpha_B - 1)}}{\frac{(c_1 + c_0) M L}{2\lambda_L^2 (\alpha_L - 1) (\alpha_B - 1)}} \\ &= \frac{\phi - p - R(c_1 + c_0) - R c_L^*}{c_L^*} \end{aligned} \tag{A.29}$$

$$\boxed{= \frac{\phi - (p + R(c_1 + c_0 - c_L^*))}{c_L^*}} \tag{A.30}$$

$$= \frac{\phi - p_L^*}{c_L^*}$$

The expression for  $p_L^*$  then is

$$\boxed{p_L^* = p + R(c_1 + c_0 - c_L^*)} \quad (\text{A.31})$$

In equation (A.29) the modified resistance  $c_L^*$  is introduced. This expression can be simplified as demonstrated below.

$$\begin{aligned} c_L^* &= \frac{(c_1 + c_0) ML}{2\lambda_L^2 (\alpha_L - 1) (\alpha_B - 1)} \\ &= \frac{L(c_1 + c_0) (\lambda_L (\alpha_L + 1) (\alpha_B - 1) - \lambda_B (\alpha_L - 1) (\alpha_B + 1))}{2\lambda_L^2 (\alpha_L - 1) (\alpha_B - 1)} \\ &= \frac{L(c_1 + c_0) \lambda_L (\alpha_L + 1) (\alpha_B - 1)}{2\lambda_L^2 (\alpha_L - 1) (\alpha_B - 1)} - \frac{L(c_1 + c_0) \lambda_B (\alpha_L - 1) (\alpha_B + 1)}{2\lambda_L^2 (\alpha_L - 1) (\alpha_B - 1)} \\ &= \frac{L(c_1 + c_0) \lambda_L (\alpha_L + 1)}{2\lambda_L^2 (\alpha_L - 1)} - \frac{L(c_1 + c_0) \lambda_B (\alpha_B + 1)}{2\lambda_L^2 (\alpha_B - 1)} \\ &= (c_0 + c_1) \frac{L}{2\lambda_L} \coth\left(\frac{L}{2\lambda_L}\right) - \frac{\lambda_B L (c_1 + c_0)}{2\lambda_L^2} \coth\left(\frac{-B}{2\lambda_B}\right) \\ &= (c_0 + c_1) \frac{L}{2\lambda_L} \coth\left(\frac{L}{2\lambda_L}\right) - \frac{L}{2} \sqrt{\frac{(c_0 + c_1)^2}{(kHc_1)^2} \frac{kHc_1c_0}{(c_0 + c_1)}} \coth\left(\frac{-B}{2\lambda_B}\right) \\ &= (c_0 + c_1) \frac{L}{2\lambda_L} \coth\left(\frac{L}{2\lambda_L}\right) - \frac{L}{2} \sqrt{\frac{c_0 (c_0 + c_1)^2}{kHc_1}} \coth\left(\frac{-B}{2\lambda_B}\right) \\ &= (c_0 + c_1) \frac{L}{2\lambda_L} \coth\left(\frac{L}{2\lambda_L}\right) - \frac{Lc_0}{B} \frac{B}{2\lambda_B} \coth\left(\frac{-B}{2\lambda_B}\right) \\ &\boxed{c_L^* = (c_0 + c_1) \frac{L}{2\lambda_L} \coth\left(\frac{L}{2\lambda_L}\right) + \frac{Lc_0}{B} \frac{B}{2\lambda_B} \coth\left(\frac{B}{2\lambda_B}\right)} \quad (\text{A.32}) \end{aligned}$$

The final step above can be made because  $\coth(x)$  is an odd function:  $f(-x) = -f(x)$ . The hyperbolic cotangent is introduced by making use of the following identity:

$$\coth(x) = \frac{\cosh(x)}{\sinh(x)} = \frac{e^x + e^{-x}}{e^x - e^{-x}} = \frac{e^{2x} + 1}{e^{2x} - 1}$$

Therefore,

$$\frac{\alpha_L + 1}{\alpha_L - 1} = \frac{\exp\left(\frac{L}{\lambda_L}\right) + 1}{\exp\left(\frac{L}{\lambda_L}\right) - 1} = \coth\left(\frac{L}{2\lambda_L}\right)$$

### A.3.2 Lumped parameters for stretch between $-B/2 \leq x \leq 0$

Similar to the previous section the average head in the top aquifer is found by integrating the solution for  $h$  (equation (A.19)) over the stretch from  $-B/2$  to 0 and dividing by the total length of that stretch.

$$\begin{aligned}
h_{av,B} &= \frac{2}{B} \int_{-B/2}^0 h_B dx \\
&= \frac{2}{B} \int_{-B/2}^0 C_{1,B} \exp\left(\frac{-x}{\lambda_B}\right) + C_{2,B} \exp\left(\frac{x}{\lambda_B}\right) + t_B dx \\
&= \frac{2}{B} \left[ -\lambda_B \alpha_B C_{2,B} \exp\left(\frac{-x}{\lambda_B}\right) + \lambda_B C_{2,B} \exp\left(\frac{x}{\lambda_B}\right) + t_B x \right]_{-B/2}^0 \\
&= \frac{2}{B} \left[ -\lambda_B \alpha_B C_{2,B} + \lambda_B C_{2,B} - \left( -\lambda_B \alpha_B C_{2,B} \exp\left(\frac{B}{2\lambda_B}\right) \right. \right. \\
&\quad \left. \left. + \lambda_B C_{2,L} \exp\left(\frac{-B}{2\lambda_B}\right) - \frac{t_B B}{2} \right) \right]
\end{aligned}$$

Because  $-\alpha_B \exp\left(\frac{B}{2\lambda_B}\right) + \exp\left(\frac{-B}{2\lambda_B}\right) = 0$  we get

$$\boxed{h_{av,B} = \frac{-2\lambda_B C_{2,B} (\alpha_B - 1)}{B} + t_B} \quad (\text{A.33})$$

Just as in the previous section we want go from the current expression (with  $h_{av,B}$ ) for the flux from the regional aquifer to the ditch to one in a form as shown on the right in the following equation. The final goal is to find expressions for  $c_B^*$  and  $p_B^*$ .

$$s_B = \frac{\phi - h_{av,B}}{c_1} \quad \rightarrow \quad s_B = \frac{\phi - p_B^*}{c_B^*}$$

Substituting  $h_{av,B}$  into leftmost equation above and using the same helper variable  $M$  defined before

$$M = \lambda_L (\alpha_L + 1) (\alpha_B - 1) - \lambda_B (\alpha_L - 1) (\alpha_B + 1)$$

$$\begin{aligned}
s_B &= \frac{\phi}{c_1} + \frac{2\lambda_B^2 (t_B - t_L) (\alpha_L - 1) (\alpha_B - 1)}{c_1 M B} - \frac{t_B}{c_1} \\
&= \frac{\phi M B + 2\lambda_B^2 (t_B - t_L) (\alpha_L - 1) (\alpha_B - 1) - t_B M B}{c_1 M B} \\
&= \frac{\frac{\phi M B}{2\lambda_B^2 (\alpha_L - 1) (\alpha_B - 1)} + t_B - t_L - \frac{t_B M B}{2\lambda_B^2 (\alpha_L - 1) (\alpha_B - 1)}}{\frac{c_1 M B}{2\lambda_B^2 (\alpha_L - 1) (\alpha_B - 1)}}
\end{aligned}$$

$$= \frac{\frac{\phi MB}{2\lambda_B^2(\alpha_L-1)(\alpha_B-1)} + \frac{c_1 p + c_0 \phi}{c_1 + c_0} - \phi + c_1 R - \frac{c_1 p + c_0 \phi}{c_1 + c_0} \frac{MB}{2\lambda_B^2(\alpha_L-1)(\alpha_B-1)}}{\frac{c_1 MB}{2\lambda_B^2(\alpha_L-1)(\alpha_B-1)}}$$

Multiplying top and bottom by  $(c_1 + c_0)$  yields:

$$= \frac{\frac{\phi MB(c_1 + c_0)}{2\lambda_B^2(\alpha_L-1)(\alpha_B-1)} + c_1 p + c_0 \phi - \phi(c_1 + c_0) + c_1 R(c_1 + c_0) - (c_1 p + c_0 \phi) \frac{MB}{2\lambda_B^2(\alpha_L-1)(\alpha_B-1)}}{\frac{c_1 MB(c_1 + c_0)}{2\lambda_B^2(\alpha_L-1)(\alpha_B-1)}}$$

Introducing another helper variable we can simplify the equation:

$$c_H = \frac{MB(c_1 + c_0)}{2\lambda_B^2(\alpha_L-1)(\alpha_B-1)}$$

$$= \frac{c_H \phi + c_1 p + c_0 \phi - c_1 \phi - c_0 \phi + c_1 R(c_1 + c_0) - \frac{c_1 p}{c_1 + c_0} c_H - \frac{c_0 \phi}{c_1 + c_0} c_H}{c_1 c_H}$$

Multiplying top and bottom again by  $(c_1 + c_0)$  we get:

$$= \frac{\phi c_H(c_1 + c_0) + p c_1(c_1 + c_0) - \phi c_1(c_1 + c_0) + R c_1(c_1 + c_0)^2 - p c_1 c_H - \phi c_0 c_H}{c_1 c_H(c_1 + c_0)}$$

$$= \frac{\phi c_H - \phi(c_1 + c_0) + p(c_1 + c_0) - p c_H + R(c_1 + c_0)^2}{c_H(c_1 + c_0)}$$

$$= \frac{\phi(c_H - c_1 - c_0) - (p(c_H - c_1 - c_0) - R(c_1 + c_0)^2)}{c_H(c_1 + c_0)}$$

$$= \frac{\phi - \left( p - \frac{R(c_1 + c_0)^2}{c_H - c_1 - c_0} \right)}{\frac{c_H(c_1 + c_0)}{c_H - c_1 - c_0}}$$

This can be rewritten in terms of  $c_L^*$  using the following relation:

$$c_H = \frac{B(c_0 + c_1)}{L c_0} c_L^*$$

Substituting in this expression for  $c_H$  yields the final answer:

$$s_B = \frac{\phi - \left( p - \frac{R(c_1 + c_0)^2}{\frac{B(c_0 + c_1)}{L c_0} c_L^* - c_1 - c_0} \right)}{\frac{\frac{B(c_0 + c_1)^2}{L c_0} c_L^*}{\frac{B(c_0 + c_1)}{L c_0} c_L^* - c_1 - c_0}} \quad (\text{A.34})$$

or:

$$s_B = \frac{\phi - p_B^*}{c_B^*}$$

where:

$$p_B^* = p - \frac{R(c_1 + c_0)^2}{\frac{B}{L} \frac{(c_0 + c_1)}{c_0} c_L^* - c_1 - c_0} \quad (\text{A.35})$$

$$c_B^* = \frac{\frac{B}{L} \frac{(c_0 + c_1)^2}{c_0} c_L^*}{\frac{B}{L} \frac{(c_0 + c_1)}{c_0} c_L^* - c_1 - c_0} \quad (\text{A.36})$$

#### A.4 Total flux between regional aquifer and ditches

To solve for the total flux that flows to or from the ditch through the bottom leaky layer, each flux is multiplied by the width of the region and added together. Dividing this result by the total width of the system we get the total flux. Expressed in a formula we get:

$$s_{tot} = \frac{s_B B + s_L L}{B + L} \quad \rightarrow \quad s_{tot} = \frac{\phi - p_{tot}^*}{c_{tot}^*}$$

Using the results found in the previous section we can rewrite  $s_{tot}$  to find expressions for lumped parameters  $p_{tot}^*$  and  $c_{tot}^*$ . The following block of algebra shows the derivation for these two values.

$$s_{tot} = \frac{B(\phi - p_B^*)}{c_B^*(B + L)} + \frac{L(\phi - p_L^*)}{c_L^*(B + L)}$$

Introducing helper variable  $Z$  and substituting in the expression for  $c_B^*$  (A.36) and multiplying top and bottom by its denominator:

$$\begin{aligned} Z &= \frac{B}{L} \frac{c_0 + c_1}{c_0} \quad (\text{A.37}) \\ &= \frac{-B\phi(c_0 + c_1 - Zc_L^*) + Bp_B^*(c_0 + c_1 - Zc_L^*)}{(B + L)(c_0 + c_1)Zc_L^*} + \frac{L\phi - Lp_L^*}{(B + L)c_L^*} \\ &= \frac{-B\phi(c_0 + c_1 - Zc_L^*) + Bp_B^*(c_0 + c_1 - Zc_L^*)}{(B + L)(c_0 + c_1)Zc_L^*} + \frac{L\phi - Lp_L^*}{(B + L)c_L^*} \cdot \frac{Z(c_0 + c_1)}{Z(c_0 + c_1)} \\ &= \frac{-B\phi(c_0 + c_1 - Zc_L^*) + Bp_B^*(c_0 + c_1 - Zc_L^*) + L\phi Z(c_0 + c_1) - Lp_L^* Z(c_0 + c_1)}{(B + L)(c_0 + c_1)Zc_L^*} \end{aligned}$$

Multiplying top and bottom by  $1/Z$ :

$$\begin{aligned}
&= \frac{-\frac{B\phi}{Z}(c_0 + c_1 - Zc_L^*) + \frac{Bp_B^*}{Z}(c_0 + c_1 - Zc_L^*) + L\phi(c_0 + c_1) - Lp_L^*(c_0 + c_1)}{(B + L)(c_0 + c_1)c_L^*} \\
&= \frac{-B\phi(\frac{c_0+c_1}{Z} - c_L^*) + \frac{Bp_B^*}{Z}(c_0 + c_1 - c_L^*) + L\phi(c_0 + c_1) - Lp_L^*(c_0 + c_1)}{(B + L)(c_0 + c_1)c_L^*}
\end{aligned}$$

Using the expression (A.37) for  $Z$ :

$$\begin{aligned}
&= \frac{-B\phi(\frac{Lc_0}{B} - c_L^*) + \frac{Bp_B^*}{Z}(c_0 + c_1 - c_L^*) + L\phi(c_0 + c_1) - Lp_L^*(c_0 + c_1)}{(B + L)(c_0 + c_1)c_L^*} \\
&= \frac{-L\phi c_0 + Bc_L^* + Lc_0\phi + Lc_1\phi + \frac{Bp_B^*}{Z}(c_0 + c_1 - c_L^*) - Lp_L^*c_0 - Lp_L^*c_1}{(B + L)(c_0 + c_1)c_L^*} \\
&= \frac{\phi(Bc_L^* + Lc_1) + \frac{Bp_B^*}{Z}(c_0 + c_1 - c_L^*) - Lp_L^*(c_0 + c_1)}{(B + L)(c_0 + c_1)c_L^*}
\end{aligned}$$

Substitution of expressions (A.31) and (A.35) for  $p_L^*$  and  $p_B^*$  respectively:

$$\begin{aligned}
&= \frac{\phi(Bc_L^* + Lc_1) + \frac{B(c_0+c_1-c_L^*)}{Z} \left( p + \frac{R(c_0+c_1)^2}{c_0+c_1-c_L^*} \right) - L(c_0 + c_1)(p + R(c_0 + c_1 - c_L^*))}{(B + L)(c_0 + c_1)c_L^*} \\
&= \frac{\phi(Bc_L^* + Lc_1) + \frac{pB}{Z}(c_0 + c_1 - c_L^*) + \frac{BR}{Z}(c_0 + c_1)^2 - Lp(c_0 + c_1) - RL(c_0 + c_1)(c_0 + c_1 - c_L^*)}{(B + L)(c_0 + c_1)c_L^*} \\
&= \frac{\phi(Bc_L^* + Lc_1) + pLc_0 - pBc_L^* - Lpc_0 - Lpc_1 + RLc_0(c_0 + c_1) - RL(c_0 + c_1)(c_0 + c_1 - c_L^*)}{(B + L)(c_0 + c_1)c_L^*} \\
&= \frac{\phi(Bc_L^* + Lc_1) - p(Bc_L^* + Lc_1) + RL(c_0 + c_1)(c_L^* - c_1)}{(B + L)(c_0 + c_1)c_L^*}
\end{aligned}$$

$$\boxed{s_{tot} = \frac{\phi - p + \frac{RL(c_0+c_1)(c_L^*-c_1)}{Bc_L^*+Lc_1}}{\frac{(B+L)(c_0+c_1)c_L^*}{Bc_L^*+Lc_1}}} \quad (\text{A.38})$$

Which is the same as:

$$s_{tot} = \frac{\phi - p_{tot}^*}{c_{tot}^*}$$

with:

$$\boxed{p_{tot}^* = p - \frac{RL(c_0 + c_1)(c_L^* - c_1)}{Bc_L^* + Lc_1}} \quad (\text{A.39})$$

$$\boxed{c_{tot}^* = \frac{(B + L)(c_0 + c_1)c_L^*}{Bc_L^* + Lc_1}} \quad (\text{A.40})$$

## Appendix B

# A cross-sectional analytic element model environment in Python

This appendix contains a brief description of the object-oriented cross-sectional multi-layer analytic element model written in Python. The solutions for the different types of elements (i.e. ditches, head-specified ditches, no-flow boundaries, areal infiltration elements, etc.) are derived in Chapter 3. The following sections give a brief description of how the solutions for the head and the potential near a ditch and a head-specified ditch are implemented in an object oriented program. The structure of the code is based on [Bakker and Kelson \(2009\)](#). For more information about the program and the actual code, contact the author.

### B.1 The Model and AquiferData classes

The `Model` class initializes an analytic element model to which analytic elements may be added. It starts out with an empty list of elements which is appended as analytic elements are added to the model. It requires the geology of the model as input, which is passed onto the `AquiferData` class where the eigenvectors and eigenvalues of the system matrix are calculated. The eigenvectors and eigenvalues are used in almost all calculations performed by the model.

The `potentialVector` method calculates the potential at any point in the cross-section for all layers in the model. It sums the potential of each individual element to calculate the total potential at that point (see Eq. 3.2). The `headVector` method uses output of `potentialVector` and translates the result to head by dividing by the transmissivity of each layer. In the actual program there are also methods for the calculation of the discharge but these are not shown here. These functions follow the same structure as

the potential functions but use the solutions for discharge given in Chapter 3.

The `solve` method is used to calculate any unknown parameters in the model, e.g. the discharge of a head-specified ditch. Elements with an unknown parameter each have a unique `equation` method that sets up the equations that need to be solved. See Section B.3 for a slightly more detailed explanation.

```
class Model:
    """Model class that sets up an analytical element model.
    All elements added to the model are stored in Model.elementList.

    Model setup:
    - See AquiferData class docstring for details of required
    parameters.
    """
    def __init__(self, Naq, k, zb, zt, c, kv=[], alpha=1.0, ctop=None,
                 cbot=None):
        self.elementList = []
        self.aq = AquiferData(Naq, k, zb, zt, c, kv, alpha, ctop, cbot)
    def potentialVector(self, x):
        p = [e.potential(x) for e in self.elementList]
        return sum(p, 0)
    def headVector(self, x):
        h = self.potentialVector(x) / Tarray
        return h
    def solve(self):
        print "Starting solve.....\nnumber of elements: "
        + str(len(self.elementList))
        self.matrix = []; self.rhsvec = [];
        for e in self.elementList:
            if e.hasunknown:
                row, rhs = e.equation()
                self.matrix.append(row)
                self.rhsvec.append(rhs)
                print "size matrix: " + str(shape(self.matrix))
        if not self.matrix:
            print "No unknowns, no need to solve!"
        else:
            sol = linalg.solve(self.matrix, self.rhsvec)
            ipar = 0
            for e in self.elementList:
                if e.hasunknown:
                    e.parameter = atleast_1d(sol[ipar])
                    ipar+=1
            print "Solution complete!\n"
```

```

class AquiferData:
    """ Base class for aquifer data.

    Input:
    - Naq: number of aquifers
    - k: list of hydraulic conductivities
    - zb: list of bottom elevations of aquifers
    - zt: list of top elevations of aquifers
    - c: list of resistances of leaky layers
    - kv: list containing vertical hydraulic conductivities.
    - alpha: anistropy factor kv/kh; default = 1.0; only used if
      no kv is given.
    - ctop: resistance of the top leaky layer; default = 1e8
    - cbot: resistance of the bottom leaky layer; default 1e30
    """
    huge = 1e30
    def __init__(self,Naq,k,zb,zt,c,kv=[],alpha=1.0,ctop=None,
    cbot=None):
        self.z = sort(list(zt) + list(zb))
        self.k = asarray(k,'d'); self.alpha = alpha;
        if len(kv)==0:
            self.kv = self.k * self.alpha
        else:
            self.kv = asarray(kv,'d')
        self.zb = asarray(zb,'d'); self.zt = asarray(zt,'d');
        self.Naq = Naq; self.H = self.zt-self.zb;
        self.T = self.H*self.k
        self.Hleakyayer = self.zb[:-1] - self.zt[1:]
        # Accounting for resistance to vertical flow in aquifers
        caq = zeros(Naq-1)
        for j in range(Naq-1):
            caq[j] = self.H[j+1]/(2*self.kv[j+1])
                + self.H[j]/(2*self.kv[j])
        caq[self.Hleakyayer!=0] += asarray(c)
        if ctop == None: ctop = 1e8
        if cbot == None: cbot = self.huge
        else: cbot += self.H[-1]/(2*self.kv[-1])
        self.c = hstack([ctop,caq,cbot])
        # Calculate the eigenvalues and eigenvectors
        self.lab,self.eigvec = self.SystemMatrix()
    def SystemMatrix(self):
        d0 = 1/(self.c[:-1]*self.T)+1/(self.c[1:]*self.T)
        dp1 = -1/(self.c[1:-1]*self.T[1:])
        dm1 = -1/(self.c[1:-1]*self.T[:-1])
        A = diag(d0,k=0) + diag(dp1,k=1) + diag(dm1,k=-1)
        (W,V) = linalg.eig(A)
        return 1/sqrt(W),V

```

## B.2 The Element base class and Ditch class

The `Element` class is the base class for all elements. All analytic element objects inherit from this class. It adds all elements to the model's element list. The `potential` method multiplies the potential influence (potential of an element when its strength is set to one) of an element by its strength (given by `self.parameter`). It performs the calculation inside the sum in (Eq. 3.2).

```
class Element:
    """ Base class for elements added to model. """
    def __init__(self,model,p):
        self.model = model
        self.parameter = p
        self.model.elementList.append(self)
        self.hasunknown = False
    def potential(self,x):
        x = atleast_1d(x)
        pinf = self.potinfo(x)
        P = empty((shape(pinf)[0],len(self.parameter),len(x)))
        for j,pinf_col in enumerate(pinf.T):
            P[:,:,j] = dot(pinf_col[newaxis].T,self.parameter[newaxis])
        return sum(P,1)
```

The ditch element is defined by the `Ditch` class. Calling this class creates a ditch object with a location `xc`, a discharge `Q` and the layer in which it is located. The `potinfo` function calculates the potential at any point in the cross-section when the discharge of the ditch is set to one.

```
class Ditch(Element):
    """Linesink element simulating ditch with fixed discharge.

    Input data:
        - model: model to which element will be added
        - xc: x-coordinate of ditch.
        - Q: Discharge per unit length in m2/d
    Optional input:
        - layers: list of layer in which element is screened
        - label: label of element added to model.elementList
    """
    def __init__(self, model, xc, Q, layers=[1], label=''):
        self.xc = array([xc], 'd')
        self.discharge = Q
        self.label = label
        self.layers = array(layers)
        self.Nscreenedlayers = len(self.layers)
        self.dischargebylayer = zeros([model.aq.Naq])
```

```

self.dischargebylayer[self.layers-1]
    = Q/(self.Nscreenedlayers)
self.q = zeros([model.aq.Naq,1])
self.q[self.layers-1] = -1/(2.*self.Nscreenedlayers)
self.an = linalg.solve(model.aq.eigvec,self.q)
self.an = squeeze(self.an) * model.aq.lab
self.type = "ditch"
Element.__init__(self,model,self.dischargebylayer)
def potinf(self,x,out=None):
    aq = self.model.aq
    x = atleast_1d(x)
    rv = zeros([aq.Naq,aq.Naq,x.shape[0]])
    for i in range(aq.Naq):
        rv[:,i,x-self.xc>=0] = dot(self.an[i] * exp(-(x[x-self.xc>=0]
            -self.xc)/aq.lab[i])[newaxis].T,aq.eigvec[:,i][newaxis]).T
        rv[:,i,x-self.xc<0] = dot(self.an[i] * exp((x[x-self.xc<0]
            -self.xc)/aq.lab[i])[newaxis].T,aq.eigvec[:,i][newaxis]).T
    return sum(rv,1)

```

### B.3 The HeadDitch and HeadEquation classes

The HeadDitch object inherits methods from the Ditch object and a special mix-in class called HeadEquation. HeadDitch requires the head to be specified instead of the discharge. It initializes a Ditch object but sets the discharge to zero. Its `self.hasunknown` attribute indicates that the discharge is unknown and needs to be calculated by the model.

The `solve` method in the Model class solves for the unknown parameter by setting up an equation like (Eq. 3.28) presented in Section 3.2.3. The equation method is defined in the HeadEquation class and returns the equation in matrix form. It returns one row of the matrix and the corresponding value for the right-hand side vector. Once the matrix and the right-hand side vector are assembled the equation is solved and the calculated strengths are assigned to their respective elements.

```

class HeadEquation:
    def equation(self):
        row = []; rhs = self.pc[self.layers-1]
        for e in self.model.elementList:
            if e.hasunknown:
                row = append(row,e.potinf(self.xc)[self.layers-1][0])
            else:
                rhs = rhs - e.potential(self.xc)[self.layers-1][0]
        return row,rhs

class HeadDitch(Ditch,HeadEquation):
    """Ditch in which head is specified. The resulting discharge is

```

*calculated by the model.*

*Input:*

- *ml: model parent*
- *xc: x-coordinate of ditch*
- *hls: head in ditch*

*Optional input:*

- *layers: list of layer in which ditch is screened*
- *label: label for element*

*"""*

```
def __init__(self,model,xc,hc,layers=[1],label=''):
    self.hc = hc
    self.pc = model.aq.T*self.hc
    self.hasunknown = True
    self.type = "headditch"
    Ditch.__init__(self,model,xc,0.0,layers=layers, label=label)
```